

Higgs Coupling Measurements and the Scale of New Physics

Fayez Abu-Ajamieh

LUPM UMR5299, Université de Montpellier, 34095 Montpellier, France

Spencer Chang

*Department of Physics and Institute for Fundamental Science
University of Oregon, Eugene, Oregon 97403*

Miranda Chen, Markus A. Luty

*Center for Quantum Mathematics and Physics (QMAP)
University of California, Davis, California 95616*

Abstract

A primary goal of present and future colliders is measuring the Higgs couplings to Standard Model (SM) particles. Any observed deviation from the SM predictions for these couplings is a sign of new physics whose energy scale can be bounded from above by requiring tree-level unitarity. In this paper, we extend previous work on unitarity bounds from the Higgs cubic coupling to Higgs couplings to vector bosons and top quarks. We find that HL-LHC measurements of these couplings compatible with current experimental bounds may point to a scale that can be explored at the HL-LHC or a next-generation collider. Our approach is completely model-independent: we assume only that there are no light degrees of freedom below the scale of new physics, and allow arbitrary values for the infinitely many couplings beyond the SM as long as they are in agreement with current measurements. We also extend and clarify the methodology of this analysis, and show that if the scale of new physics is above the TeV scale, then the deviations can be described by the leading higher-dimension gauge invariant operator, as in the SM effective field theory.

1 Introduction

The discovery of the Higgs boson at the Large Hadron Collider (LHC) has opened a new chapter in elementary particle physics. For the first time, we have an experimentally established theory of particle physics that can be consistently extrapolated to energy scales many orders of magnitude larger than what we can hope to directly probe experimentally. On the other hand, there is no doubt that there is new physics beyond the Standard Model (SM): neutrino masses, dark matter, the matter-antimatter asymmetry, and inflation all cannot be explained by the SM. In addition, there are serious conceptual problems with the SM, most importantly the absence of a natural explanation of the electroweak scale and the cosmological constant. Although there can be little doubt that the SM is not the ultimate theory of nature, none of these open questions unambiguously point to a scale that can be probed in future experiments.

The situation was very different before the experimental discovery of the Higgs boson. Unitarity arguments indicated that the theory of electroweak interactions is incomplete without a Higgs sector at or below the TeV scale. It was established in the 1970s that unitarity of amplitudes at high energy requires the theory to be a spontaneously broken gauge theory [1–4] (see [5–7] for a modern approach). Lee, Quigg, and Thacker [8, 9] turned this into a quantitative constraint, showing that tree-level unitarity of longitudinal vector boson scattering could be used to give a bound on the energy scale of the Higgs sector (see also Refs. [10–13]). This bound was a major motivation for the Large Hadron Collider (LHC), which indeed discovered the Higgs boson in the predicted mass range.

A very important part of the continuing high-energy collider program is the experimental study of the newly-discovered Higgs boson. The Higgs boson is unlike any other elementary particle: it has spin 0 and no other quantum numbers that distinguish it from the vacuum. The Higgs mass has been measured at the percent level, and if the SM is assumed to be correct, this fixes all the parameters of the theory to high accuracy. On the other hand, the couplings of a single Higgs boson to other SM fields have been measured only at the 20% level, while the coupling of the Higgs to itself is only bounded to be $\lesssim 10$ times the SM prediction. Because the parameters of the SM have already been determined much more accurately, measurements of the Higgs couplings are best viewed as a search for physics beyond the SM.

All this is well known. However, what is often not sufficiently emphasized is that if these measurements find a deviation from the SM predictions, then they directly point to a scale of new physics, in exactly the same way that the work of Lee, Quigg, and Thacker pointed to the scale of the Higgs sector before its discovery. The reason is that the SM is the unique UV complete theory with the observed particle content. This means that any deviation from the SM can only be explained by either new light degrees of freedom or new interactions that ruin the UV completeness of the theory. This UV incompleteness shows up in violations of

tree-level unitarity, just as for the SM without the Higgs. Tree-level unitarity violation is a sign of strong coupling in the UV, which requires new physics at or below that scale.

As our results will show, upcoming HL-LHC measurements of Higgs couplings probe new physics at the scale of a few TeV or below. This scale is not sufficiently large that we can confidently neglect higher-dimension operators in the Standard Model effective field theory (SMEFT). Therefore, in this paper we adopt a completely model-independent approach to the interpretation of the measurements of Higgs couplings. We describe these couplings by the following effective Lagrangian in unitary gauge:

$$\begin{aligned}
\mathcal{L} = & \mathcal{L}_{\text{SM}} - \delta_3 \frac{m_h^2}{2v} h^3 - \delta_4 \frac{m_h^2}{8v^2} h^4 - \sum_{n=5}^{\infty} \frac{c_n}{n!} \frac{m_h^2}{v^{n-2}} h^n + \dots \\
& + \delta_{Z1} \frac{m_Z^2}{v} h Z^\mu Z_\mu + \delta_{W1} \frac{2m_W^2}{v} h W^{\mu+} W_\mu^- + \delta_{Z2} \frac{m_Z^2}{2v^2} h^2 Z^\mu Z_\mu + \delta_{W2} \frac{m_W^2}{v^2} h^2 W^{\mu+} W_\mu^- \\
& + \sum_{n=3}^{\infty} \left[\frac{c_{Zn}}{n!} \frac{m_Z^2}{v^n} h^n Z^\mu Z_\mu + \frac{c_{Wn}}{n!} \frac{2m_W^2}{v^n} h^n W^{\mu+} W_\mu^- \right] + \dots \\
& - \delta_{t1} \frac{m_t}{v} h \bar{t} t - \sum_{n=2}^{\infty} \frac{c_{tn}}{n!} \frac{m_t}{v^n} h^n \bar{t} t + \dots
\end{aligned} \tag{1.1}$$

Here \mathcal{L}_{SM} is the SM Lagrangian, h is the real scalar field that parameterizes the physical Higgs boson (with $\langle h \rangle = 0$), Z_μ , W_μ^\pm are the SM gauge fields, and t is a Dirac spinor field parameterizing the top quark. The δ parameters parameterize deviations in couplings that are already present in the SM, while the c parameters denote additional couplings that are not present in the SM.¹ The ellipses denote terms with additional derivatives and/or powers of the SM fields. The parameters in \mathcal{L}_{SM} are measured at the percent level or better by precision measurements of electroweak processes and the mass of the Higgs boson. The parameters δ_{V1} and δ_{t1} are currently constrained at the 20% level, while δ_3 , δ_{V2} , and c_{t2} are more weakly constrained. These couplings will be measured with significant improvements in accuracy at the upcoming HL-LHC run as well as at future colliders, motivating the focus on these couplings. As already mentioned above, any deviation from the SM predictions in these measurements is a sign of physics beyond the SM and points to a scale of new physics that can be explored experimentally. To do this, we assume that there are no additional particles below some UV scale E_{max} , and determine E_{max} by requiring that the theory satisfies tree-level unitarity up to the scale E_{max} .

The implications of unitarity for extensions of the SM has been extensively studied, but there are a number of new features to the present analysis.

- We use a completely model-independent bottom-up approach. In particular, we do not make any assumption about the infinitely many unconstrained couplings in Eq. (1.1)

¹The δ parameters in Eq. (1.1) are directly related to the κ parameters used in experimental determinations of Higgs boson couplings [14], e.g. $\kappa_Z = 1 + \delta_{Z1}$ and $\kappa_t = 1 + \delta_{t1}$.

other than that they are compatible with existing measurements. For example, we allow cancelations among measured and unmeasured couplings. In this way, we obtain unitarity constraints that are valid independently of these parameters, and show that marginalizing over them conservatively does not substantially improve the bounds.

- Previous work has focused on unitarity constraints on $2 \rightarrow 2$ partial wave amplitudes [8–11, 15, 16] and inclusive cross sections [12, 13, 17–19]. We follow Ref. [20] and directly impose unitarity constraints on dimensionless $n \rightarrow m$ amplitudes that are generalizations of $2 \rightarrow 2$ partial wave amplitudes. With this technique, we obtain unitarity bounds that can be numerically stronger than those found in previous analyses. In addition, these amplitudes have interesting properties, *e.g.* potential IR enhancements and disconnected contributions, that merit further investigation.
- We discuss the interplay between different SM deviations in determining the scale of new physics. For example, the dominant unitarity-violating process arising from δ_{t1} also depends on δ_{V1} . More phenomenologically, double Higgs production constrains a combination of δ_3 , δ_{V2} , and c_{t2} , and we work out the constraints on the scale of new physics in this expanded parameter space.
- Without assuming any effective Lagrangian power counting scheme, we show that if the scale of new physics is much larger than the TeV scale, the deviations are well-described by the leading higher-dimension gauge invariant operators, as in SMEFT. We give quantitative estimates of the errors of the SMEFT predictions purely from unitarity.

The outline of this paper is as follows. In §2 we consider the Higgs cubic coupling, extending the results of Ref. [20] in several ways. First, we use this as an example to give a more detailed discussion of the model-independence of the unitarity bound and the effective field theory framework we use to obtain it. We then show that marginalizing over unmeasured couplings does not substantially improve the unitarity bound, and we show that if the scale of new physics is high, the quartic Higgs coupling is approximately described by the predictions of the Standard Model effective field theory. In §3 and §4 we analyze these same questions for the hVV and $h\bar{t}t$ couplings, respectively. In these cases, we find that measurements at HL-LHC that are consistent with current constraints may point to a scale of new physics in the few TeV range, a scale that can be directly explored at the HL-LHC and future colliders. In §5, we consider the couplings $hhVV$ and $hh\bar{t}t$, which can also be probed by future colliders, and show that upcoming measurements of these couplings can also point to new physics at the few TeV scale. In §6 we summarize our conclusions, and an Appendix gives details of our calculation techniques and a summary of the calculations used in the main text.

2 New Physics from the Higgs Self-Coupling

In this section we discuss the model-independent bound on the scale of new physics from measurements of the cubic Higgs self-coupling. This section is based on Ref. [20], but goes beyond it in a number of respects. First, we include a more complete discussion of the model-independence of the bound and the role of additional deviations from the SM that are poorly constrained. Specifically, we explain why couplings with additional derivatives and powers of gauge fields do not affect the bounds. We also show that marginalizing over the infinitely unmeasured couplings does not substantially improve the bound. Second, we show that if the scale of unitarity violation is large compared to 1 TeV, unitarity alone implies that the deviation in the Higgs quartic coupling is related to that of the Higgs cubic coupling as predicted by the dimension-6 operator $(H^\dagger H)^3$. We are able to give a quantitative estimate of the error purely from bottom-up considerations.

2.1 Model-Independent Bound on the Scale of New Physics

Suppose that the experimentally measured value of the Higgs cubic coupling differs from the prediction of the SM. Obviously, this implies that there is physics beyond the SM, but at what scale? One possibility is that this physics is near the electroweak scale, for example additional Higgs bosons that mix with the observed Higgs boson. In this case, the new states can be potentially produced and observed in direct searches. But it is also possible that the new physics responsible for the deviation is at higher energies that are not directly probed by current experiments. Because the SM is the unique UV complete theory with the observed particle content, the scale of this new physics cannot be arbitrarily high. One sign of this is that any effective theory that can explain this result without the addition of new light particles violates tree-level unitarity at high energies. This scale can be computed without any additional assumptions, and gives an upper bound on the scale of new physics.

In a theory without gauge interactions, a cubic scalar interaction is a relevant coupling whose effects are small at high energies. Nonetheless, a deviation of the Higgs cubic coupling from the SM prediction implies a breakdown of tree-level unitarity at high energies. For example, this can be seen in the process $V_L V_L V_L \rightarrow V_L V_L V_L$, where V_L is a longitudinally polarized W or Z . This has a tree-level contribution from the Higgs cubic coupling, as shown in Fig. 1. By itself, this contributes to dimensionless amplitudes² with high-energy behavior $\sim E^2/v^2$, which would violate unitarity at high energy, but in the SM this diagram cancels with other diagrams to give high-energy behavior that respects unitarity. If the Higgs cubic coupling deviates from the SM prediction, this cancellation is destroyed, and the amplitude violates unitarity at high energies.

²We use amplitudes that are many-particle generalizations of partial wave amplitudes normalized so that the unitarity bound is $|\hat{\mathcal{M}}| < 1$. See Appendix A for details.

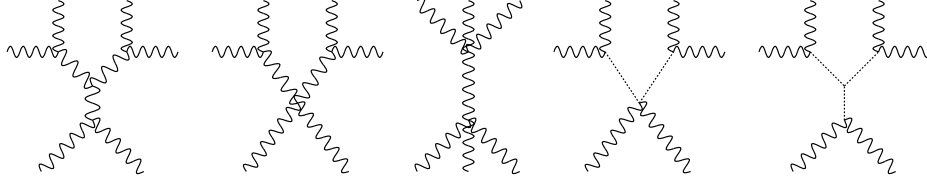


Fig. 1. Feynman diagrams contributing to scattering processes involving six electroweak gauge bosons.

The scale of unitarity violation depends on the high-energy behavior of the amplitude. The calculation of this can be considerably simplified using the equivalence theorem, which tells us that the leading high-energy behavior of scattering amplitudes for longitudinally polarized gauge bosons is given by the amplitude for the corresponding ‘eaten’ Nambu-Goldstone bosons [4, 21]. We assume that experiments can be described by the effective Lagrangian Eq. (1.1), with no new degrees of freedom below some energy scale $E_{\text{max}} \gtrsim \text{TeV}$. In this section, we focus on the couplings δ_3 and δ_4 in Eq. (1.1), which parameterize the deviations of the Higgs cubic and quartic couplings coupling from the SM values:

$$\delta_3 = \frac{g_{h^3} - g_{h^3}^{(\text{SM})}}{g_{h^3}^{(\text{SM})}}, \quad \delta_4 = \frac{g_{h^4} - g_{h^4}^{(\text{SM})}}{g_{h^4}^{(\text{SM})}}, \quad (2.1)$$

while the c_n parameters in Eq. (1.1) are couplings that are not present in the SM.

The Lagrangian Eq. (1.1) is written in unitary gauge. To use the equivalence theorem to compute the leading high-energy behavior of amplitudes, we must restore the dependence on the Nambu-Goldstone fields. We do this by writing the Higgs doublet in a general gauge as

$$H = \frac{1}{\sqrt{2}} \begin{pmatrix} G^1 + iG^2 \\ v + h + iG^3 \end{pmatrix}, \quad (2.2)$$

where $\vec{G} = (G^1, G^2, G^3)$ parameterizes the custodial $SU(2)$ triplet of ‘eaten’ Nambu-Goldstone bosons. We use a linear parameterization of the Nambu-Goldstone fields because the SM part of the Lagrangian has manifestly good high-energy behavior when written in terms of these fields. To use the equivalence theorem, we must restore the dependence on the Nambu-Goldstone of the non-SM couplings in Eq. (1.1). We do this by writing them in terms of the Higgs doublet Eq. (2.2):

$$X \equiv \sqrt{2H^\dagger H} - v = h + \frac{\vec{G}^2}{2(v+h)} - \frac{\vec{G}^4}{8(v+h)^3} + O\left(\frac{\vec{G}^6}{(v+h)^5}\right). \quad (2.3)$$

Because $X = h$ in unitary gauge, the generalization of Eq. (1.1) to a general gauge is obtained simply by the substitution $h \rightarrow X$ [19, 20]. Note that X is non-analytic at $H = 0$, but we are interested in the expansion around $\langle H \rangle \neq 0$.

The X^3 term contains interactions with arbitrarily high powers of the fields h and \vec{G} . However, such vertices also get contributions from terms of the form X^n with $n \geq 4$, and these terms are unconstrained experimentally. In order to obtain a bound we call our *model-independent bound*, we only consider processes that do not get corrections from the unmeasured couplings δ_n for $n \geq 4$. From Eq. (2.3) we have

$$\begin{aligned}
X^3 &\sim h^3 + \vec{G}^2(h^2 + h^3 + \dots) + \vec{G}^4(h + h^2 + \dots) + \vec{G}^6(1 + h + \dots) \\
&\quad + \vec{G}^8(1 + h + \dots) + \vec{G}^{10}(1 + h + \dots) + \dots, \\
X^4 &\sim h^4 + \vec{G}^2(h^3 + h^4 + \dots) + \vec{G}^4(h^2 + h^3 + \dots) + \vec{G}^6(h + h^2 + \dots) \\
&\quad + \vec{G}^8(1 + h + \dots) + \vec{G}^{10}(1 + h + \dots) + \dots, \\
X^5 &\sim h^5 + \vec{G}^2(h^4 + h^5 + \dots) + \vec{G}^4(h^3 + h^4 + \dots) + \vec{G}^6(h^2 + h^3 + \dots) \\
&\quad + \vec{G}^8(h + h^2 + \dots) + \vec{G}^{10}(1 + h + \dots) + \dots.
\end{aligned} \tag{2.4}$$

where we have set $v = 1$ and ignored numerical factors. We note that the $h\vec{G}^4$ and \vec{G}^6 couplings violate unitarity at high energies, and are not affected by the unconstrained terms X^n for $n \geq 4$. We see that the unitarity-violating amplitudes that depend only on δ_3 are (restoring factors of v)

$$\hat{\mathcal{M}}(V_L V_L \rightarrow V_L V_L h) \sim \lambda \delta_3 \frac{E}{v}, \quad \hat{\mathcal{M}}(V_L V_L V_L \rightarrow V_L V_L V_L) \sim \lambda \delta_3 \frac{E^2}{v^2}. \tag{2.5}$$

The strongest constraint comes from $W_L^+ W_L^+ W_L^- \rightarrow W_L^+ W_L^+ W_L^-$ and gives the bound

$$E_{\max} \simeq \frac{14 \text{ TeV}}{|\delta_3|^{1/2}}. \tag{2.6}$$

For details of the calculations, see Ref. [20] and the Appendix of this paper.

Experimental sensitivity to a deviation in the Higgs cubic coupling comes mainly from measurements of di-Higgs production.³ However, a deviation in this process can also be explained by new physics contributions to the $h^2 V^2$ or $h^2 \bar{t} t$ couplings. This will be discussed in §5 below, where we show that a model-independent unitarity bound can be obtained by considering these couplings together.

2.2 Model-Independence of the Bound

We claim that the bound Eq. (2.6) is valid independently of the infinitely many unconstrained couplings that parameterize possible deviations from the SM. In this subsection, we discuss this point in more detail.

The discussion above has assumed that a measured deviation in the Higgs trilinear coupling is explained by a h^3 coupling with no derivatives. (The same assumption is made by

³It is also possible to constrain a cubic deviation by looking for the hV^4 process in VBF production of hV^2 [22].

the experimental searches for this deviation.) However, there are infinitely many derivative couplings that can contribute to an observed deviation in the Higgs cubic coupling:

$$\Delta\mathcal{L} = \sum_{n=1}^{\infty} c_{3,n} \frac{m_h^2}{v^{2n+1}} \partial^{2n} h^3. \quad (2.7)$$

Here we have only shown the schematic dependence of the derivatives, but not the detailed Lorentz structure. If the experimentally measured h^3 coupling deviates from the Standard Model prediction, this is potentially due to some combination of the $c_{3,n}$ couplings above. If the deviation is dominated by a single coupling $c_{3,n}$, this requires

$$\frac{\delta g_{h^3}}{g_{h^3}^{(\text{SM})}} \sim c_{3,n} \left(\frac{m_h}{v} \right)^{2n}, \quad (2.8)$$

since the Higgs coupling extraction is dominated at energies $\sim m_h$. The $V_L^3 \rightarrow V_L^3$ process leads to a unitarity violating scale (neglecting order one numerical factors)

$$E_{\text{max}} \sim m_h \left(\frac{128\pi^3 v^4}{m_h^4} \frac{g_{h^3}^{(\text{SM})}}{\delta g_{h^3}} \right)^{1/(2n+2)}. \quad (2.9)$$

If one takes $\delta g_{h^3}/g_{h^3}^{(\text{SM})} \sim \delta_3$ to compare with the earlier bound Eq. (2.6), one finds the unitarity bound gets more stringent with increasing n and thus interpreting a Higgs trilinear deviation with the operator with the fewest derivatives leads to the most conservative new physics bound.

An important assumption in the argument above is that the number of derivatives in an operator determines its scaling with energy. In particular, we assume that each additional derivative give an additional factor of $\partial \sim E$ in scattering amplitudes at high energy. This is what is expected in general, but it can fail in certain choices of operator basis. This is because field redefinitions and integration by parts in the effective Lagrangian do not affect scattering amplitudes, so there are ‘flat directions’ in the space of effective Lagrangians. For example, the field redefinition $h \rightarrow h - (\delta_3/2v)h^2$ can be used to eliminate the deviation in the h^3 coupling, but will induce correlated couplings of the form $h^2\Box h$, h^2V^2 and $h^2\bar{t}t$. In this basis, the $h^2\Box h$, h^2V^2 couplings typically lead to E^4 growth in the V_L^6 amplitude as expected from counting derivatives, but with the correlated values induced by the field redefinition the leading growth is canceled, resulting in the same E^2 growth as the original h^3 deviation. Thus, a basis which eliminates h^3 is a poor basis for our purposes, since it obscures the energy scaling through non-trivial cancellations. To our knowledge, it has never been proven that there exists a basis where the naïve energy scaling holds, even though this assumption is commonly used in applications of effective field theory. In this paper we will assume that such a basis exists, and leave further investigation of this point for future work.⁴

⁴A natural guess is that this basis can be defined using amplitude methods [5, 23], where the connection between the number of derivatives and the energy scaling of amplitudes is manifest.

Since the unitarity bound Eq. (2.6) comes from scattering of gauge bosons, we must also consider effective couplings involving gauge fields. For example, from the unitary-gauge diagrams shown in Fig. 1 we can see that a deviation in the hV^2 and h^2V^2 couplings can also give rise to unitarity violation in the V_L^6 amplitude at high energy. The hV^2 and h^2V^2 couplings are phenomenologically interesting in their own right, and will be studied in detail in §3 and §5 respectively below. Here we preview some of the results of §3 to understand how modifications of the hV^2 and h^2V^2 couplings contribute to the V_L^6 amplitude. To use the equivalence theorem, we restore the Nambu-Goldstone bosons in the gauge boson fields in unitary gauge (see Eq. (3.3) below):

$$gV_\mu \rightarrow gV_\mu + \frac{\partial_\mu G}{v} + \frac{h\partial_\mu G}{v^2} + \dots, \quad (2.10)$$

where g is the gauge coupling. This gives (temporarily setting $v = 1$)

$$\begin{aligned} X(gV)^2 &\sim \partial^2[\vec{G}^2(h + h^2 + \dots) + \vec{G}^4(1 + h + \dots) + \vec{G}^6(1 + h + \dots) + \dots], \\ X^2(gV)^2 &\sim \partial^2[\vec{G}^2(h^2 + h^3 + \dots) + \vec{G}^4(h + h^2 + \dots) + \vec{G}^6(1 + h + \dots) + \dots], \\ X^3(gV)^2 &\sim \partial^2[\vec{G}^2(h^3 + h^4 + \dots) + \vec{G}^4(h^2 + h^3 + \dots) + \vec{G}^6(h + h^2 + \dots) + \dots]. \end{aligned} \quad (2.11)$$

Here we have assumed custodial symmetry so that the Nambu-Goldstones appear in a custodial singlet \vec{G}^2 . These give a contribution to the V_L^6 amplitude (restoring the factors of v)

$$\Delta\hat{\mathcal{M}}(V_L V_L V_L \rightarrow V_L V_L V_L) \sim (\delta_{V1} + \delta_{V2}) \frac{E^4}{v^4}, \quad (2.12)$$

where δ_{V1} and δ_{V2} are defined in Eq. (1.1) and their coefficients in the above equation are only schematic. We see that deviations in the hV^2 and h^2V^2 couplings contribute to the amplitude the same way as higher-derivative couplings at high energy, and therefore they can only lower the scale of unitarity violation. Similar results hold for modifications of the V^3 and V^4 couplings, as well as terms with additional derivatives. These give contributions to the V_L^6 amplitude that grow even faster with energy, and therefore do not invalidate the bound Eq. (2.6).

To determine the unitarity bounds from a Higgs cubic coupling deviation, we conservatively assume that δ_{V1} , δ_{V2} , and higher-derivative couplings are zero and focus on the δ_3 coupling. Contributions to the amplitude that are higher order in δ_3 involve propagators that give additional $1/E^2$ suppression at high energies, so the leading unitarity violation is given by a single insertion of δ_3 even for $\delta_3 \gtrsim 1$.⁵

⁵For other processes, we will find that the leading contributions to the unitarity bound include diagrams with propagators, for example Eq. (4.5).

2.3 The Optimal Bound

The bound Eq. (2.6) makes no assumption about the nature of the new physics other than that it is at high scales, and is valid independently of the values of the infinitely many unmeasured couplings δ_4, c_n in Eq. (1.1). However, it is not guaranteed this is the best possible bound, because it does not take the effects of all possible unmeasured couplings into account. The reason is the following. If we allow additional unmeasured couplings to be nonzero, these predict additional higher-body processes that depend on δ_3 as well as the unmeasured couplings. Requiring that these additional processes do not violate unitarity below the scale Eq. (2.6) places additional constraints on these couplings.⁶ It is possible that there is no choice of the new couplings that satisfies the unitarity bound Eq. (2.6), in which case we obtain a stronger unitarity bound. In other words, an optimal bound is obtained by marginalizing over the unmeasured couplings, while the bound Eq. (2.6) is independent of these couplings.

We have not found a general method to obtain the optimal bound. However, in the case of the V_L^6 amplitude we can constrain the optimal bound to show that it does not significantly improve the bound Eq. (2.6). To do this, we consider a theory consisting of the SM plus the dimension-6 interaction $(H^\dagger H)^3$. This corresponds to a particular choice of the higher dimension X^n operators that includes terms only up to six scalars (see Eq. (2.2)). Therefore, for this choice of couplings we can simply check all unitarity violating processes and put a bound on the scale of unitarity violation. The optimal bound will always be weaker than the unitarity violating scale obtained from the $(H^\dagger H)^3$ theory, since this corresponds to a particular choice for the infinitely many unconstrained couplings. If this scale is the same as Eq. (2.6), we will know that this is the optimal bound; if not, we learn that the optimal bound is between the bound Eq. (2.6) and the one just described.

We find that the strongest bound in the $(H^\dagger H)^3$ theory comes from the V_L^6 amplitude for small values of δ_3 , but for larger values the process $hh \rightarrow hhh$ dominates and gives

$$E_{\max} \simeq \frac{32 \text{ TeV}}{|\delta_3|}. \quad (2.13)$$

The results are plotted in Fig. 2. The scale of tree-level unitarity violation is an estimate for the scale of strong coupling, and is therefore subject to theoretical uncertainty. As a rough parameterization of this uncertainty, we vary the constraint from $\frac{1}{2} < |\mathcal{M}| < 2$. Within this range, we see that there is no important difference between the model-independent bound and the optimal bound.

⁶In fact, we know that at least some of these couplings must be nonzero, because the theory with only $\delta_3 \neq 0$ violates unitarity at the TeV scale [19, 20].

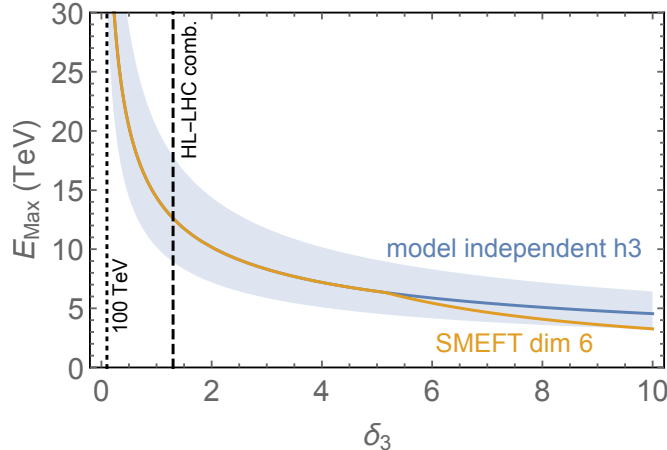


Fig. 2. The unitarity bound as a function of the deviation in the h^3 coupling. The optimal bound lies between the model-independent and SMEFT estimates. The band around the model-independent scale reflects the uncertainty of the bound from varying the unitarity constraint to $\frac{1}{2} \leq |\hat{\mathcal{M}}| \leq 2$. For comparison, we show projected 95% C.L. limits on δ_3 from a combination at HL-LHC and a 100 TeV pp collider from [24].

2.4 SMEFT Predictions from Unitarity

If the scale of new physics is high, we expect that the new physics must be of the decoupling type. This means that the effects of the new physics at low energies can be captured by adding to the SM a series of higher-dimension gauge-invariant operators. This is the SMEFT framework. If experiments reveal a deviation in one or more SM measurements, without any sign of new physics, it is most natural to interpret the results in terms of SMEFT.

SMEFT is predictive because the same SMEFT operator controls more than one observable. However, these predictions assume that we can neglect higher-dimension terms, and the size of these corrections is unknown without further theoretical input. We now show that we can make an interesting quantitative statement about this purely from unitarity considerations. Specifically, we show that if the scale of new physics is much larger than the TeV scale, we can bound the error of the SMEFT prediction, and this error bound gets better as the scale of new physics gets larger.

To be specific, we assume that $\delta_3 \neq 0$, and the energy scale of new physics is lower than some value E_{max} . In this case, we expect that the observed deviation in the Higgs cubic coupling can be explained by the dimension-6 SMEFT operator⁷

$$\delta\mathcal{L}_{\text{SMEFT}} = \frac{1}{M^2} \left(H^\dagger H - \frac{v^2}{2} \right)^3. \quad (2.14)$$

⁷Technically, this operator is a linear combination of dimension 0, 2, 4 and 6 operators, but we will refer to these linear combinations by their highest dimension.

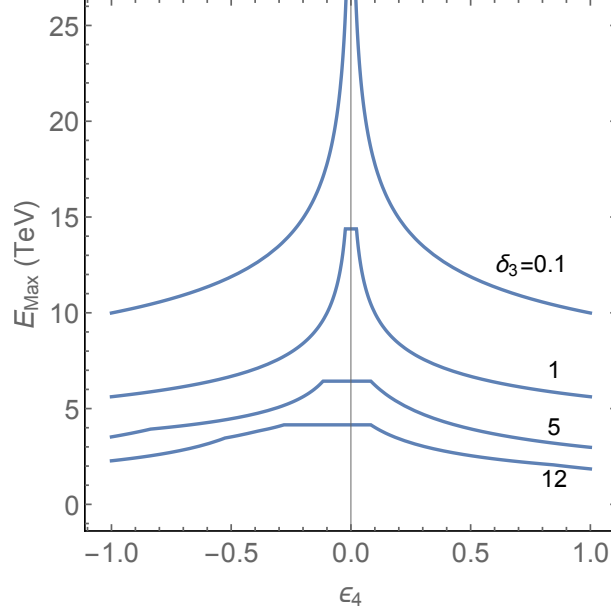


Fig. 3. Unitarity violating scales from processes that depend on δ_3 and δ_4 as a function of the fractional deviation ϵ_4 from the dimension-6 SMEFT prediction (see Eqs. (2.15) and (2.16)).

This form of the operator keeps the Higgs mass and electroweak VEV at their tree level values, but modifies the Higgs mass parameter and quartic coupling. If this operator dominates, it predicts

$$\delta_3 = \frac{2v^4}{M^2 m_h^2}, \quad \delta_4 = 6\delta_3, \quad c_5 = c_6 = 45\delta_3. \quad (2.15)$$

We expect these predictions to become more accurate if the scale of new physics is larger since these additional couplings themselves generate new unitarity violating amplitudes which require coupling correlations to be canceled.

To make this quantitative, we simply require that any deviation in the quartic coupling does not give rise to tree-level unitarity violation below the scale E_{\max} . This requirement not only bounds the quartic coupling from being too large, but it also predicts that its deviation must be close to the prediction of the dimension-6 SMEFT operator Eq. (2.14):

$$\epsilon_4 = \frac{\delta_4 - \delta_4^{\text{dim } 6}}{\delta_4^{\text{dim } 6}} \ll 1. \quad (2.16)$$

The reason for this is that adding a X^4 term to the effective Lagrangian means that there are now additional processes that violate unitarity, which are not affected by couplings of the form X^n with $n \geq 5$. The one that is most sensitive to new physics is the process $W_L^+ W_L^+ W_L^- W_L^- \rightarrow W_L^+ W_L^+ W_L^- W_L^-$, which gives the bound

$$E_{\max} \simeq \frac{8.7 \text{ TeV}}{|\delta_4 - 6\delta_3|^{1/4}}. \quad (2.17)$$

The denominator vanishes for $\delta_4 = 6\delta_3$ because the SMEFT operator does not contain a \tilde{G}^8 term. Requiring that the theory violates unitarity above some scale that is large compared to 1 TeV therefore requires that the deviations are close to the SMEFT prediction $\delta_4 = 6\delta_3$. Taking into account all of the processes predicted by the X^3 and X^4 couplings, the results are shown in Fig. 3. For example, we see that for $E_{\text{max}} \sim 10$ TeV, the deviation in the quartic coupling is within $\sim 10\%$ of the value predicted by dimension-6 SMEFT. This shows that not finding new physics below some scale can be complementary to direct searches [25–27] in constraining the quartic coupling.

3 New Physics from hVV Couplings

The Higgs couplings to vector bosons $V = W^\pm, Z$ provides another sensitive probe for new physics. In this section, we work out the model-independent constraints on the scale of new physics from measurements of these couplings. Note that we will not consider Higgs coupling to massless gauge bosons, which can be probed by $h \rightarrow \gamma\gamma, Z\gamma, gg$. These lie outside the thrust of this paper because they do not lead to high-energy growth in V_L scattering. Also, because these couplings are loop-induced in the Standard Model, we expect that deviations from the Standard Model predictions will give rather weak unitarity constraints.

3.1 Model-Independent Bound on the Scale of New Physics

It is well known that a deviation in the hVV couplings leads to unitarity violation in longitudinal W and Z scattering at high energies (see [8, 9] and more recently [28]). In the SM, the Higgs exchange contribution cancels the E^2 growth of other diagrams, so any modification of the hVV coupling will ruin this cancellation and lead to unitarity violation. We can reproduce this result using the same model-independent bottom-up approach we used for the h^3 coupling. We write down the most general deviations from the SM involving the Higgs and vector bosons that are quadratic in the W and Z gauge boson fields:

$$\begin{aligned} \mathcal{L} = \mathcal{L}_{\text{SM}} - \alpha\delta T \left(\frac{1}{2}m_Z^2 Z^\mu Z_\mu \right) + \delta_{Z1} \frac{m_Z^2}{v} h Z^\mu Z_\mu + \delta_{W1} \frac{2m_W^2}{v} h W^{\mu+} W_\mu^- \\ + \delta_{Z2} \frac{m_Z^2}{2v^2} h^2 Z^\mu Z_\mu + \delta_{W2} \frac{m_W^2}{v^2} h^2 W^{\mu+} W_\mu^- + c_{Z3} \frac{m_Z^2}{3!v^3} h^3 Z^\mu Z_\mu + \dots, \end{aligned} \quad (3.1)$$

where h is the scalar field that parameterizes the physical Higgs boson (see Eq. (2.2)). As before, we do not assume any power counting for the higher terms, we only assume that their values are compatible with experimental constraints. Our bounds are obtained by marginalizing over the values of the infinitely many unmeasured couplings. For now, we do not assume that custodial symmetry is preserved by the deviations from the SM, and therefore we have included an additional contribution to the T parameter from shifting the Z mass.

To understand the implications of the couplings in Eq. (3.1) for processes involving longitudinally polarized vectors at high energy, we use the equivalence theorem. To do this, we write the new couplings in Eq. (3.1) in terms of gauge invariant operators using

$$\hat{H} = \frac{H}{\sqrt{H^\dagger H}} = \begin{pmatrix} 0 \\ 1 \end{pmatrix} + O(\vec{G}). \quad (3.2)$$

This transforms under electroweak gauge symmetry just like a Higgs doublet. This allows us to write the vector fields in terms of gauge-invariant operators:

$$\begin{aligned} \hat{H}^\dagger i D_\mu \hat{H} &= -\frac{m_Z}{v} Z_\mu - \frac{1}{v} \partial_\mu G^0 + \dots, \\ \tilde{\hat{H}}^\dagger i D_\mu \hat{H} &= \frac{\sqrt{2} m_W}{v} W_\mu^+ + \frac{i\sqrt{2}}{v} \partial_\mu G^+ + \dots, \\ \hat{H}^\dagger i D_\mu \tilde{\hat{H}} &= \frac{\sqrt{2} m_W}{v} W_\mu^- - \frac{i\sqrt{2}}{v} \partial_\mu G^- + \dots, \end{aligned} \quad (3.3)$$

where we have defined

$$\tilde{\hat{H}} = \epsilon \hat{H}^*, \quad \epsilon = \begin{pmatrix} 0 & 1 \\ -1 & 0 \end{pmatrix}. \quad (3.4)$$

We then use Eq. (3.3) to write Eq. (3.1) as a sum of gauge invariant operators. We therefore have

$$\mathcal{L} = \mathcal{L}_{\text{SM}} - \frac{\alpha v^2 \delta T}{2} |\hat{H}^\dagger D_\mu \hat{H}|^2 + \delta_{Z1} v X |\hat{H}^\dagger D_\mu \hat{H}|^2 + \delta_{W1} v X |\tilde{\hat{H}}^\dagger D_\mu \hat{H}|^2 + \dots, \quad (3.5)$$

where X is defined in Eq. (2.3). We can now expand this expression in powers of the Nambu-Goldstone fields \vec{G} and Higgs field h using

$$\begin{aligned} \hat{H} &= \left(1 + \frac{\vec{G}^2}{(v+h)^2} \right)^{-1/2} \begin{pmatrix} \frac{\sqrt{2} G^+}{v+h} \\ 1 + i \frac{G^0}{v+h} \end{pmatrix} \\ &= \begin{pmatrix} 0 \\ 1 \end{pmatrix} + \frac{1}{v+h} \begin{pmatrix} \sqrt{2} G^+ \\ i G^0 \end{pmatrix} - \frac{\vec{G}^2}{2(v+h)^2} \begin{pmatrix} 0 \\ 1 \end{pmatrix} + O(\vec{G}^3). \end{aligned} \quad (3.6)$$

The only model-independent couplings arising from δT , δ_{Z1} and δ_{W1} are then

$$\begin{aligned} \delta \mathcal{L} &= \frac{\alpha \delta T + \delta_{Z1}}{v} h \partial^\mu G^0 \partial_\mu G^0 + \frac{2 \delta_{W1}}{v} h \partial^\mu G^+ \partial_\mu G^- + \frac{\alpha \delta T}{v} (\partial_\mu h \partial^\mu G^0) G^0 \\ &+ \frac{i \alpha \delta T}{v} \partial_\mu G^0 (G^- \partial^\mu G^+ - G^+ \partial^\mu G^-) + \frac{\alpha \delta T}{2 v^2} (G^+ \partial_\mu G^- - G^- \partial_\mu G^+)^2 \\ &+ \frac{2 \alpha \delta T + \delta_{Z1}}{2 v^2} (\vec{G})^2 \partial^\mu G^0 \partial_\mu G^0 + \frac{\delta_{W1}}{v^2} (\vec{G})^2 \partial^\mu G^+ \partial_\mu G^- \\ &+ \frac{i}{v^2} [(3 \alpha \delta T - 2 \delta_{W1} + 2 \delta_{Z1}) h \partial^\mu G^0 + \alpha \delta T G^0 \partial^\mu h] (G^+ \partial_\mu G^- - G^- \partial_\mu G^+) \\ &+ \frac{i}{v^3} (2 \alpha \delta T - \delta_{W1} + \delta_{Z1}) (\vec{G})^2 \partial^\mu G^0 (G^+ \partial_\mu G^- - G^- \partial_\mu G^+). \end{aligned} \quad (3.7)$$

Interactions involving higher powers of Nambu-Goldstone or Higgs fields can be generated by next order couplings such as δ_{Z2} and δ_{W2} , which are much less constrained experimentally. Notice that the δT term contributes to these interactions at the same order as δ_{Z1}, δ_{W1} . However, given the stringent experimental constraints on the T parameter, $\alpha\delta T \lesssim 0.001$, these effects are subdominant because we are considering significantly larger deviations $\delta_{Z1}, \delta_{W1} \sim 0.1$, so we will often neglect δT in the following discussion.⁸

The unitarity constraints on δ_{Z1} and δ_{W1} come from the amplitudes $V_L V_L \rightarrow V_L h, V_L V_L \rightarrow V_L V_L$, and $V_L V_L V_L \rightarrow V_L V_L$. These get contributions from a contact term from Eq. (3.7) while the last two also have a contribution from a Higgs exchange giving the schematic form:

$$\begin{aligned}\hat{\mathcal{M}}(V_L V_L \rightarrow V_L h) &\sim (\delta_{V1}) \frac{E^2}{v^2}, \\ \hat{\mathcal{M}}(V_L V_L \rightarrow V_L V_L) &\sim (\delta_{V1} + \delta_{V1}^2) \frac{E^2}{v^2}, \\ \hat{\mathcal{M}}(V_L V_L V_L \rightarrow V_L V_L) &\sim (\delta_{V1} + \delta_{V1}^2) \frac{E^3}{v^3}.\end{aligned}\tag{3.8}$$

Because of the experimental constraint $|\delta_{V1}| \lesssim 0.2$, we neglect the quadratic terms. The processes that give the strongest constraints are:

$$\begin{aligned}W_L^+ W_L^+ \rightarrow W_L^+ W_L^+ : E_{\max} &\simeq \frac{1.2 \text{ TeV}}{|\delta_{W1}|^{1/2}}, \\ Z_L Z_L \rightarrow W_L^+ W_L^- : E_{\max} &\simeq \frac{1.5 \text{ TeV}}{|\delta_{Z1} + \delta_{W1}|^{1/2}}, \\ W_L^+ h \rightarrow W_L^+ Z_L : E_{\max} &\simeq \frac{1.0 \text{ TeV}}{|\delta_{Z1} - \delta_{W1}|^{1/2}}, \\ W_L^+ W_L^+ W_L^- \rightarrow W_L^+ Z_L : E_{\max} &\simeq \frac{1.5 \text{ TeV}}{|\delta_{Z1} - \delta_{W1}|^{1/3}}.\end{aligned}\tag{3.9}$$

There are no unitarity constraints depending on δ_{Z1} alone. This is because the $ZZ \rightarrow ZZ$ amplitude does not grow at high energies, since it is proportional to $s + t + u = 4m_Z^2$. Note that a measured deviation on one or both of these couplings of order of the current 2σ bounds $|\delta_{Z1}|, |\delta_{W1}| \sim 0.2$ would imply new physics below a few TeV, a scale that can be explored at the HL-LHC itself. We plot the strongest bounds from Eq. (3.9) in Fig. 4, together with the ATLAS limits on δ_{Z1} and δ_{W1} [30] and the HL-LHC projections [24]. Notice that $\delta_{Z1} = \delta_{W1}$ (the positive diagonal on the plot) corresponds to the custodial symmetry limit which has weaker unitarity bounds than the maximally custodial violating direction $\delta_{Z1} = -\delta_{W1}$, due to the last two processes in Eq. (3.9).

⁸Ref. [29] recently pointed out that the $W_L W_L Z_L h$ amplitude violates unitarity only if custodial symmetry is broken. This can be verified by the fourth line in Eq. (3.7). From the last line, we see that this also extends to the $Z_L W_L^4$ and $Z_L^3 W_L^2$ amplitudes.

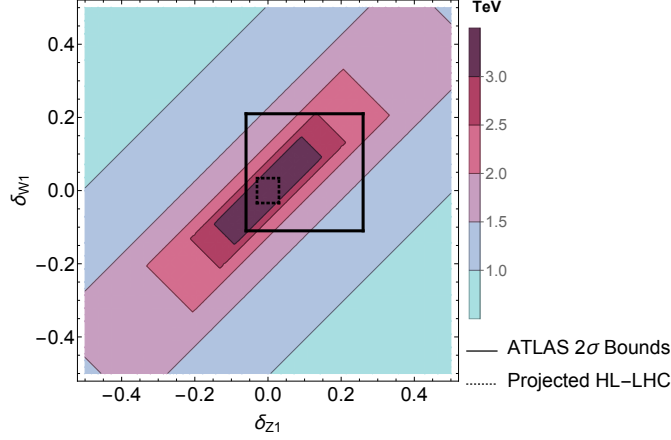


Fig. 4. The unitarity-violating scale that depends on δ_{Z1} and δ_{W1} assuming that custodial symmetry is not preserved. The solid black line represents the current ATLAS 95% C.L. constraints [30] while the dotted black line gives the HL-LHC projections [24].

3.2 Optimal Bound with Custodial Symmetry

As emphasized in §2.1, bounds such as Eq. (3.9) make no assumptions about the nature of the new physics other than that it is at high scales, and are valid independently of the values of the infinitely many unmeasured couplings. However, as discussed in §2.3, marginalizing over these unmeasured couplings may give a stronger bound, which we call the optimal bound. In this section we show that if we assume that the new physics preserves custodial symmetry, the model-independent bound from Eq. (3.9) is in fact optimal. We will discuss the case without custodial symmetry in §3.4 below.

We focus on the custodial symmetry limit where $\delta T = 0$ and $\delta_{W1} = \delta_{Z1} \equiv \delta_{V1}$. This limit is well-motivated by the strong experimental bounds on the T parameter. We consider the dimension-6 SMEFT operator

$$\delta\mathcal{L}_{\text{SMEFT}} = \frac{1}{M^2} \left(H^\dagger H - \frac{v^2}{2} \right) |D_\mu H|^2. \quad (3.10)$$

This does not contribute to the T parameter, and gives a custodial symmetry preserving deviation to the hVV couplings. Making a field redefinition to remove the momentum-dependent terms $h\partial h^2$ and $h^2\partial h^2$, we find that this operator predicts

$$\delta_{V1} = \frac{v^2}{2M^2}, \quad \delta_{V2} = 4\delta_{V1}, \quad c_{V3} = 8\delta_{V1}, \quad c_{V4} = 8\delta_{V1}, \quad (3.11)$$

where $\delta_{V2} = \delta_{Z2} = \delta_{W2}$, and $c_{Vn} = 0$ for $n \geq 5$. Using this, we can calculate the additional amplitudes predicted by Eq. (3.10) that violate unitarity, namely $h^2 Z_L^2$ and $h^2 W_L^2$ and check whether these give a lower scale of unitarity violation for a given value of δ_{V1} . We find that

these new processes give weaker or equivalent bounds to the model-independent bound for $\delta_{Z1} = \delta_{W1}$,

$$E_{\max} \simeq \frac{1.1 \text{ TeV}}{|\delta_{V1}|^{1/2}}, \quad (3.12)$$

which is therefore also the optimal bound in this case. This is shown in Fig. 5 along with the constraints from ATLAS and a HL-LHC projection, showing the potential to constrain new physics below ~ 5 TeV.

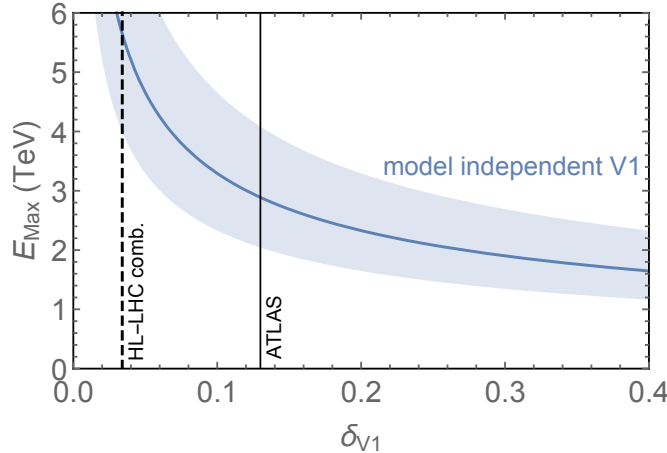


Fig. 5. The unitarity bound as a function of the deviation in the hVV coupling. The optimal bound lies between the model-independent and SMEFT estimate from the dimension-6 operator Eq. (3.10) and thus they are the same. The band around the model-independent scale results from varying the unitarity bound to $\frac{1}{2} \leq |\hat{\mathcal{M}}| \leq 2$. For comparison, we show the 95% C.L. limits on δ_{V1} from ATLAS [30] and a projected HL-LHC combination [24].

3.3 SMEFT Predictions from Unitarity with Custodial Symmetry

If the scale of new physics is high, we expect that an observed deviation in the Higgs couplings can be described by the lowest-dimension SMEFT operator. In this section we assume that the new physics preserves custodial symmetry, and consider the question of the accuracy of the SMEFT prediction, following the logic explained in §2.4. The dimension-6 SMEFT operator Eq. (3.10) predicts $\delta_{V2} = 4\delta_{V1}$, and we define

$$\epsilon_{V2} \equiv \frac{\delta_{V2} - \delta_{V2}^{\text{dim } 6}}{\delta_{V2}^{\text{dim } 6}}. \quad (3.13)$$

When we include both δ_{V1} and δ_{V2} , we have the additional model-independent processes $hh \rightarrow V_L V_L$, $hV_L V_L \rightarrow V_L V_L$ and $V_L V_L V_L \rightarrow V_L V_L V_L$. Requiring that these do not violate unitarity constrains E_{\max} for a given value of ϵ_{V2} . The results are shown in Fig. 6. The

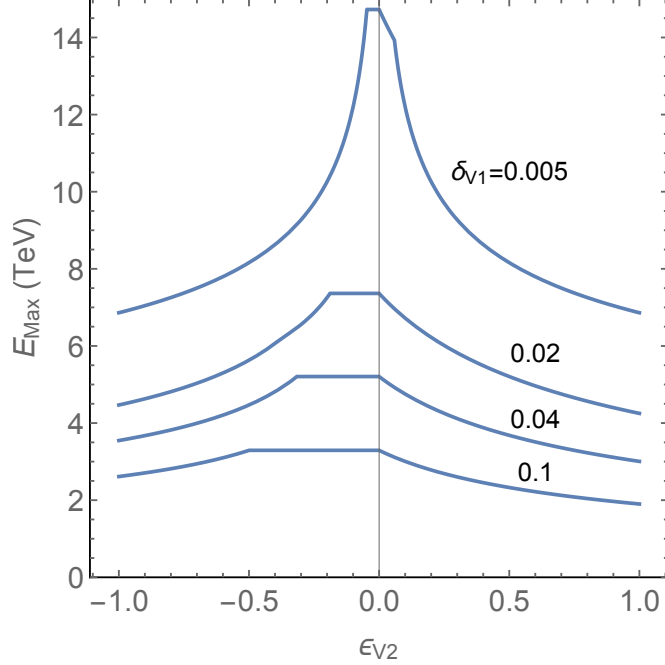


Fig. 6. Unitarity violating scales from processes that depend on δ_{V1} and δ_{V2} as a function of the fractional deviation of δ_{V2} from its SMEFT prediction, $\delta_{V2} = 4\delta_{V1}(1 + \epsilon_{V2})$.

results are qualitatively similar to the case of the Higgs self-interaction. The predictions of SMEFT become accurate for $E_{\text{max}} \gtrsim 10$ TeV, corresponding to values of δ_{V1} much smaller than what will be probed in upcoming experiments, and since the unitarity-violating scale is low even for δ_{V1} of $O(1\%)$, in this case a general value of δ_{V2} does not change the bound much.

3.4 Optimal Bound Without Custodial Symmetry

We now consider the unitarity bounds for the case $\delta_{Z1} \neq \delta_{W1}$. This case is somewhat unnatural, in the sense that for values of δ_{Z1} and δ_{W1} that violate custodial symmetry at a level that is observable in upcoming experiments, the small observed T parameter appears to require an unnatural cancellation. Nonetheless, δ_{Z1} and δ_{W1} will be independently measured, and it is interesting to explore the implications of $\delta_{Z1} \neq \delta_{W1}$.

For concreteness we consider the case $\delta_{Z1} \neq 0$, $\delta_{W1} \simeq 0$, $\alpha\delta T \simeq 0$. In order to explain this in SMEFT, we must introduce the dimension-8 operator

$$\frac{1}{M^4} \left(H^\dagger H - \frac{v^2}{2} \right) |H^\dagger D_\mu H|^2, \quad (3.14)$$

which has been chosen so that $\delta T = 0$. This operator predicts the following coupling

deviations:

$$\begin{aligned}
\delta_{Z1} &= \frac{v^4}{4M^4}, & \delta_{W1} &= 0, & \delta_{Z2} &= 8\delta_{Z1}, & \delta_{W2} &= -\delta_{Z1}, \\
c_{Z3} &= 40\delta_{Z1}, & c_{W3} &= -8\delta_{Z1}, & c_{Z4} &= 136\delta_{Z1}, & c_{W4} &= -32\delta_{Z1}, \\
c_{Z5} &= 288\delta_{Z1}, & c_{W5} &= -72\delta_{Z1}, & c_{Z6} &= 288\delta_{Z1}, & c_{W6} &= -72\delta_{Z1}.
\end{aligned} \tag{3.15}$$

There are now many more unitarity-violating amplitudes, and the unitarity violating scale that we obtain assuming that the dimension-8 operator dominates is somewhat stronger than the model-independent bound. The results are shown in Fig. 7.

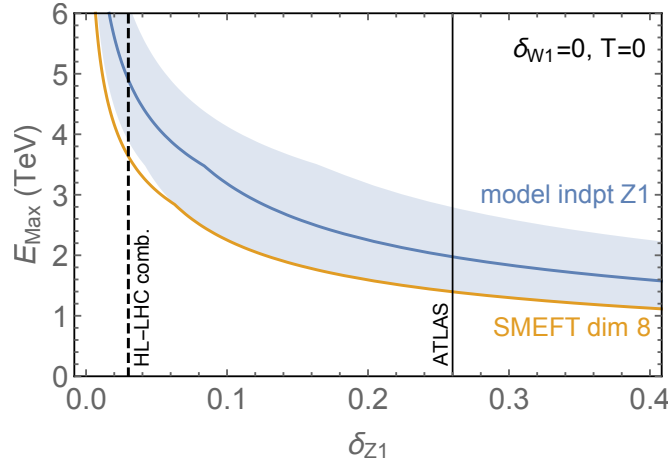


Fig. 7. The unitarity bound as a function of the deviation in the hZZ coupling, assuming $\delta_{W1} = 0$, $\delta T = 0$. The optimal bound lies between the model-independent and SMEFT estimate from the dimension-8 operator Eq. (3.14). The band around the model-independent scale results from varying the unitarity bound to $\frac{1}{2} \leq |\hat{M}| \leq 2$. For comparison, we show the 95% C.L. limits on δ_{Z1} from ATLAS [30] and a projected HL-LHC combination [24].

4 New Physics from $h\bar{t}t$ Couplings

The Higgs couplings to top quarks $h\bar{t}t$ provides another sensitive probe of new physics. In this section we work out the model-independent constraints on the scale of new physics from measurements of this coupling.

4.1 Model-Independent Bound

If the $h\bar{t}t$ coupling deviates from the SM value, processes such as $t\bar{t} \rightarrow W_L^+ W_L^-$ will violate unitarity at high energy. This observation goes back to Ref. [10], which put a bound on the scale of fermion mass generation in a theory without a Higgs boson. The diagrams

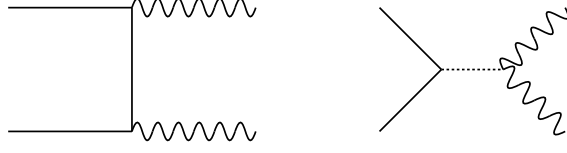


Fig. 8. Feynman diagrams contributing to $t\bar{t} \rightarrow W_L^+ W_L^-$ in unitary gauge.

contributing to this process in unitary gauge are shown in Fig. 8. We see that they are sensitive to both the $\bar{t}th$ coupling and the hVV coupling, and we will see that the unitarity bound depends on both δ_{t1} and δ_{V1} in Eq. (1.1). Unitarity violation for more general top couplings in $2 \rightarrow 2$ processes has been recently studied in [31, 32].

As in the previous sections, we use the equivalence theorem to compute the high-energy behavior of amplitudes involving longitudinally polarized vector bosons and Higgs fields. We do this by writing the deviations from the SM in Eq. (1.1) that depend on the top quark in a general gauge:

$$\delta\mathcal{L} = -m_t(\bar{Q}_L\tilde{H}t_R + \text{h.c.}) \left(\delta_{t1}\frac{X}{v} + c_{t2}\frac{X^2}{2!v^2} + \dots \right), \quad (4.1)$$

where X is given by Eq. (2.3) and \tilde{H} is given by Eqs. (3.2) and (3.4). Expanding these terms in terms of the Higgs and Nambu-Goldstone bosons gives

$$\bar{Q}_L\tilde{H}t_R + \text{h.c.} = \frac{1}{\sqrt{1 + \frac{\vec{G}^2}{(v+h)^2}}} \left(\bar{t}t - \frac{1}{v+h} \left[G^0\bar{t}i\gamma_5 t + \sqrt{2}G^-\bar{b}_L t_R + \sqrt{2}G^+\bar{t}_R b_L \right] \right). \quad (4.2)$$

This leads to the following interaction pattern (temporarily setting $v = 1$)

$$\begin{aligned} \bar{t}tX &\sim tt^c[h + iG^0(h + \dots) + \vec{G}^2(1 + \dots) + iG^0\vec{G}^2(1 + \dots) + \vec{G}^4(1 + \dots) + \dots] \\ &\quad + bt^cG^+[(h + \dots) + \vec{G}^2(1 + \dots) + \vec{G}^4(1 + \dots) + \dots] + \text{h.c.}, \\ \bar{t}tX^2 &\sim tt^c[h^2 + iG^0(h^2 + \dots) + \vec{G}^2(h + \dots) + iG^0\vec{G}^2(h + \dots) + \vec{G}^4(1 + \dots) + \dots] \\ &\quad + bt^cG^+[(h^2 + \dots) + \vec{G}^2(h + \dots) + \vec{G}^4(1 + \dots) + \dots] + \text{h.c.}, \\ \bar{t}tX^3 &\sim tt^c[h^3 + iG^0(h^3 + \dots) + \vec{G}^2(h^2 + \dots) + iG^0\vec{G}^2(h^2 + \dots) + \vec{G}^4(h + \dots) + \dots] \\ &\quad + bt^cG^+[(h^3 + \dots) + \vec{G}^2(h^2 + \dots) + \vec{G}^4(h + \dots) + \dots] + \text{h.c.}, \end{aligned} \quad (4.3)$$

where the parentheses allow arbitrary higher powers of h . Examining the structure of the interactions in Eq. (4.3), we see that the model-independent couplings that depend only on δ_{t1} are

$$\begin{aligned} \delta\mathcal{L} \supset & -\delta_{t1}\frac{m_t}{v} \left[\left(h + \frac{1}{2v}\vec{G}^2 \right) \bar{t}t - \left(h + \frac{1}{2v}\vec{G}^2 \right) \frac{G^0}{v}\bar{t}i\gamma_5 t \right] \\ & + \delta_{t1}\frac{\sqrt{2}m_t}{v^2} \left[\left(h + \frac{1}{2v}\vec{G}^2 \right) G^-\bar{b}_L t_R + \text{h.c.} \right]. \end{aligned} \quad (4.4)$$

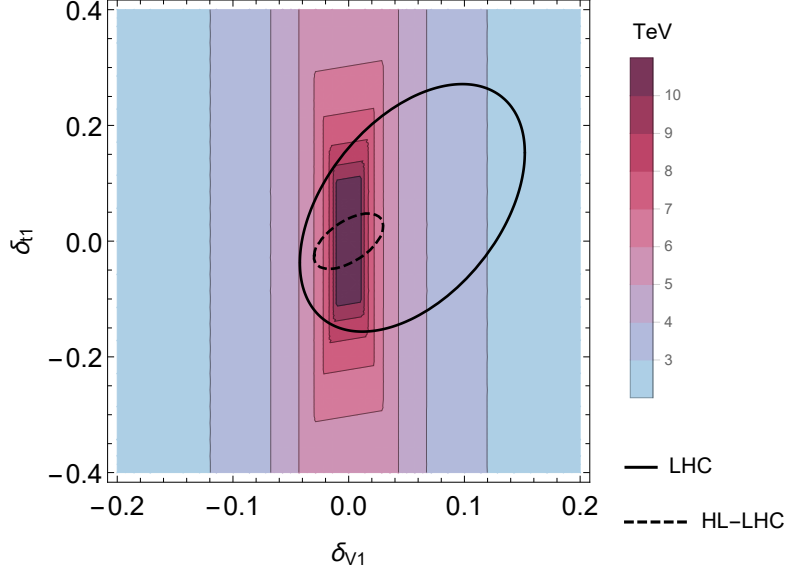


Fig. 9. Unitarity violating scales given values of δ_{t1} and δ_{V1} . The solid line represents the 95% C.L. at the LHC [30] and the dashed line is the HL-LHC projection for ATLAS [33].

As discussed previously in §2.2, we can also consider tth interactions with additional derivatives, but again we expect these will give a parametrically lower scale of unitarity violation, and therefore in terms of new physics bounds, it is conservative to interpret a tth coupling deviation in terms of the coupling with no derivatives. We can then determine the schematic form for the following model-independent amplitudes:

$$\begin{aligned}
 \hat{\mathcal{M}}(\bar{q}q \rightarrow V_L V_L) &\sim y_t (\delta_{t1} + \delta_{V1} + \delta_{t1}\delta_{V1}) \frac{E}{v}, \\
 \hat{\mathcal{M}}(\bar{q}q \rightarrow V_L h) &\sim y_t (\delta_{t1} + \delta_{V1}) \frac{E}{v}, \\
 \hat{\mathcal{M}}(\bar{q}q \rightarrow V_L V_L V_L) &\sim y_t (\delta_{t1} + \delta_{V1} + \delta_{t1}\delta_{V1} + \delta_{V1}^2) \frac{E^2}{v^2},
 \end{aligned} \tag{4.5}$$

where $q = t, b$. For the $\bar{b}t$ initial state processes, the first process vanishes. Amplitudes related to these by crossing have the same scaling. The terms depending on δ_{V1} arise from diagrams with propagators (see Eq. (3.7)). The 2 derivatives in vertices from δ_{V1} cancel the energy suppression of the extra propagators, so these contributions are the same order. For contributions with a propagator, there is a possibility of $\log(E/m)$ terms arising from the phase space integrals in the amplitudes. By direct calculation, we show that these are absent in all of the terms in Eq. (4.5), except possibly for the δ_{V1}^2 term in the last line. This contribution is numerically small even if a log is present, and so we will neglect all quadratic contributions.

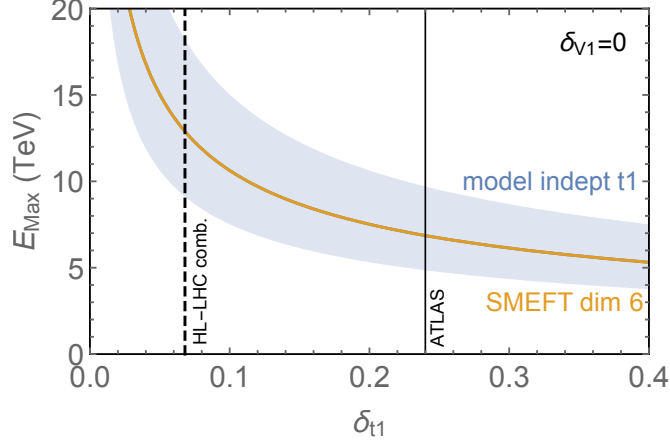


Fig. 10. The unitarity bound on δ_{t1} assuming $\delta_{W1}, \delta_{Z1} = 0$. The model-independent bound is equal to the optimal bound for all values of δ_{t1} shown. The band around the model-independent scale results from varying the unitarity bound to $\frac{1}{2} \leq |\hat{\mathcal{M}}| \leq 2$. For comparison, we show the 95% C.L. limits on the coupling from ATLAS [30] and a projected HL-LHC combination [24].

The best bounds on δ_{t1} from these processes are

$$\begin{aligned}
t_R \bar{t}_R \rightarrow W_L^+ W_L^- : E_{\max} &\simeq \frac{5.1 \text{ TeV}}{|\delta_{t1} + \delta_{V1}|}, \\
t_R \bar{b}_R \rightarrow W_L^+ h : E_{\max} &\simeq \frac{3.6 \text{ TeV}}{|\delta_{t1} - \delta_{V1}|}, \\
t_R \bar{b}_R \rightarrow W_L^+ W_L^+ W_L^- : E_{\max} &\simeq \frac{3.3 \text{ TeV}}{\sqrt{|\delta_{t1} - \frac{1}{3}\delta_{V1}|}},
\end{aligned} \tag{4.6}$$

where we assume custodial symmetry $\delta_{Z1} = \delta_{W1} = \delta_{V1}$. As already mentioned above, these bounds are numerically stronger than previous bounds [10, 12, 13].

Fig. 9 shows the unitarity violating scale from these processes as a function of δ_{t1} and δ_{V1} , together with projected HL-LHC constraints on these couplings. From this graph, we see that upcoming measurements of δ_{V1} are sensitive to lower scales of new physics. However, if measurements of hVV agree with the SM, a deviation in the $h\bar{t}t$ coupling at HL-LHC that is compatible with current constraints can still point to a scale of new physics below 8 TeV.

4.2 Optimal Bound

To further discuss the implications of δ_{t1} , we consider a scenario where δ_{t1} is nonzero, but all the other Higgs couplings are compatible with the SM. To estimate the scale of new physics in this scenario, it is conservative to assume $\delta_{W1}, \delta_{Z1} = 0$, since unitarity bounds from Eq. (3.9) are stronger than Eq. (4.1). As in previous sections, we consider the optimal bound obtained

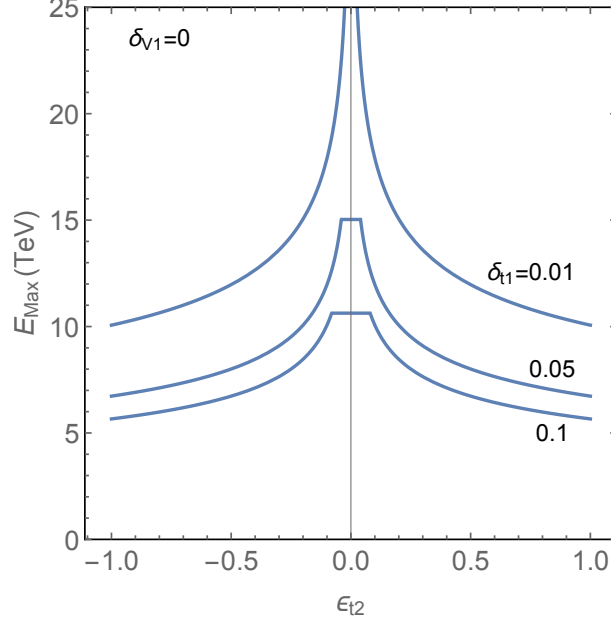


Fig. 11. The unitarity bound from processes that depend on δ_{t1} , $c_{t2} = 3\delta_{t1}(1 + \epsilon_{t2})$ where $\epsilon_{t2} = 0$ is the prediction of the dimension-6 SMEFT operator. Due to these amplitudes depending on coupling δ_{V1} , it has been set to zero in this plot.

by marginalizing over the infinitely many unmeasured couplings. The optimal bound can be constrained by considering the SMEFT operator

$$\delta\mathcal{L}_{\text{SMEFT}} = \frac{y_t}{M^2} \left(H^\dagger H - \frac{v^2}{2} \right) (\bar{Q}_L \tilde{H} t_R + \text{h.c.}), \quad (4.7)$$

which gives

$$\delta_{t1} = -\frac{v^2}{M^2}, \quad c_{t2} = c_{t3} = 3\delta_{t1}, \quad (4.8)$$

and $c_{tn} = 0$ for $n \geq 4$. This imposes additional unitarity bounds. We find that the bounds for the model-independent processes considered above give the most stringent bound for small δ_{t1} , but for larger values of δ_{t1} the strongest bound comes from $\bar{t}_R t_R \rightarrow hh$, which gives

$$E_{\text{max}} \simeq \frac{2.4 \text{ TeV}}{|\delta_{t1}|}. \quad (4.9)$$

However, this only dominates over the bounds in Eq. (4.1) for $\delta_{t1} \gtrsim 0.6$, which is larger than allowed by current constraints. In Fig. 10 we show the unitarity bounds on δ_{t1} along with the experimental bounds from ATLAS and the projected sensitivity of a HL-LHC combination.

4.3 SMEFT Predictions from Unitarity

If the scale of new physics is high, we expect that an observed deviation in the Higgs couplings can be described by the lowest-dimension SMEFT operator. In the case of the $\bar{t}th$ coupling, this is the operator given in Eq. (4.7), which makes the predictions Eq. (4.8) for the higher-order deviations. We can constrain the accuracy of these predictions from unitarity, as outlined in previous sections. The results are shown in Fig. 11. As expected, the SMEFT predictions are accurate only if the scale of new physics is $\gtrsim 10$ TeV.

5 New Physics from $hhVV$ and $hh\bar{t}t$ Couplings

In this section we discuss the implications of a deviation in the $hhVV$ or $hh\bar{t}t$ coupling, parameterized respectively by δ_{V2} and c_{t2} in Eq. (1.1). Since there are no symmetries to prevent this, any new physics that contributes to these couplings should also contribute to a comparable deviation in δ_{V1} and δ_{t1} , which will be measured to greater precision. On the other hand, it is possible that δ_{V1} and δ_{t1} are suppressed by an accidental cancellation. In any case, experimental constraints on δ_{V2} and c_{t2} will improve dramatically at the HL-LHC, and will give us additional information about possible new physics. Another motivation for studying these couplings is that they directly contribute to di-Higgs production. Therefore, an anomalous rate for di-Higgs production may be due to δ_{V2} (in vector boson fusion) or δ_{t2} (from gluon fusion). Therefore we should consider these couplings in order to determine the unitarity bounds from any future di-Higgs anomalies.

5.1 $hhVV$: Model-Independent Bound on the Scale of New Physics

We now work out the model-independent bound on the scale of new physics coming from an observation of $\delta_{V2} \neq 0$. This coupling can be measured from di-Higgs production via vector boson fusion [34]. Although this process in principle is sensitive to an anomaly in the h^3 coupling, this sensitivity is strongly reduced by requiring large di-Higgs invariant mass to suppress backgrounds. Because any new physics that contributes to δ_{V2} will also contribute to δ_{V1} , we assume that both couplings are nonzero in the present discussion.

The procedure we use to obtain the model-independent bound is an extension of the one used in §3 to include $\delta_{V2} \neq 0$. This adds the model-independent processes $h^2V_L^2$, hV_L^4 , and V_L^6 . Because the δ_{V1} and δ_{V2} couplings each contain 2 derivatives additional insertions of these vertices can cancel the $1/E^2$ from additional propagators. This means that the leading

diagrams at high energy include diagrams with multiple propagators. We find

$$\begin{aligned}
\hat{\mathcal{M}}(V_L V_L \rightarrow hh) &\sim (\delta_{V1} + \delta_{V2} + \delta_{V1}^2) \frac{E^2}{v^2}, \\
\hat{\mathcal{M}}(V_L V_L \rightarrow V_L V_L h) &\sim (\delta_{V1} + \delta_{V2} + \delta_{V1}^2 + \delta_{V1} \delta_{V2} + \delta_{V1}^3) \frac{E^3}{v^3}, \\
\hat{\mathcal{M}}(V_L V_L V_L \rightarrow V_L V_L V_L) &\sim (\delta_{V1} + \delta_{V2} + \delta_{V1}^2 + \delta_{V1} \delta_{V2} + \delta_{V1}^2 \delta_{V2} + \delta_{V1}^3 + \delta_{V1}^4) \frac{E^4}{v^4}.
\end{aligned} \tag{5.1}$$

Amplitudes related to these by crossing have the same scaling. Current experimental constraints give $|\delta_{V1}| \lesssim 0.2$, while δ_{V2} has a weak constraint of $-1.8 \leq \delta_{V2} \leq 1.9$ at 95% C.L. [35]. We can therefore neglect the nonlinear terms in these amplitudes (which are also much more difficult to compute). Assuming custodial symmetry ($\delta_{Z1} = \delta_{W1}$, $\delta_{Z2} = \delta_{W2}$) the strongest bounds are

$$\begin{aligned}
W_L^+ W_L^- \rightarrow hh : \quad E_{\max} &\simeq \frac{1.5 \text{ TeV}}{|\delta_{V2} - 2\delta_{V1}|^{1/2}}, \\
Z_L Z_L \rightarrow h W_L^+ W_L^- : \quad E_{\max} &\simeq \frac{1.9 \text{ TeV}}{|\delta_{V2} - 4\delta_{V1}|^{1/3}}, \\
W_L^+ W_L^+ Z_L \rightarrow W_L^+ W_L^+ Z_L : \quad E_{\max} &\simeq \frac{2.6 \text{ TeV}}{|\delta_{V2} - 4\delta_{V1}|^{1/4}}.
\end{aligned} \tag{5.2}$$

In Fig. 12, we show the unitarity violating scale given values of δ_{V1} and δ_{V2} along with the bounds on both coupling deviations from standard searches and a search for vector boson fusion di-Higgs. The figure shows that HL-LHC searches for VBF di-Higgs could find coupling deviations with unitarity bounds below 3 TeV.

5.2 $hhVV$: Optimal Bound and SMEFT Predictions

We now consider the optimal bound obtained by marginalizing over the infinitely many unmeasured couplings. As in previous sections, we do this by considering a scenario where these couplings are given by a single SMEFT operator. In the present case, we use the dimension-8 operator

$$\frac{1}{M^4} \left(H^\dagger H - \frac{v^2}{2} \right)^2 D^\mu H^\dagger D_\mu H, \tag{5.3}$$

which gives custodial symmetry preserving couplings. Performing field redefinitions to remove the Higgs self couplings at order $1/M^4$, we have find that the Higgs couplings to the vector bosons are given by

$$\delta_{V1} = 0, \quad \delta_{V2} = \frac{v^4}{M^4}, \quad c_{V3} = 8\delta_{V2}, \quad c_{V4} = 32\delta_{V2}, \quad c_{V5} = 72\delta_{V2}, \quad c_{V6} = 72\delta_{V2}, \tag{5.4}$$

and $c_{Vn} = 0$ for $n \geq 7$. The unitarity bound obtained from this operator is always stronger than the optimal bound, so the optimal bound lies between this bound and the model-independent bound computed above. In Fig. 13, we plot both the model-independent and

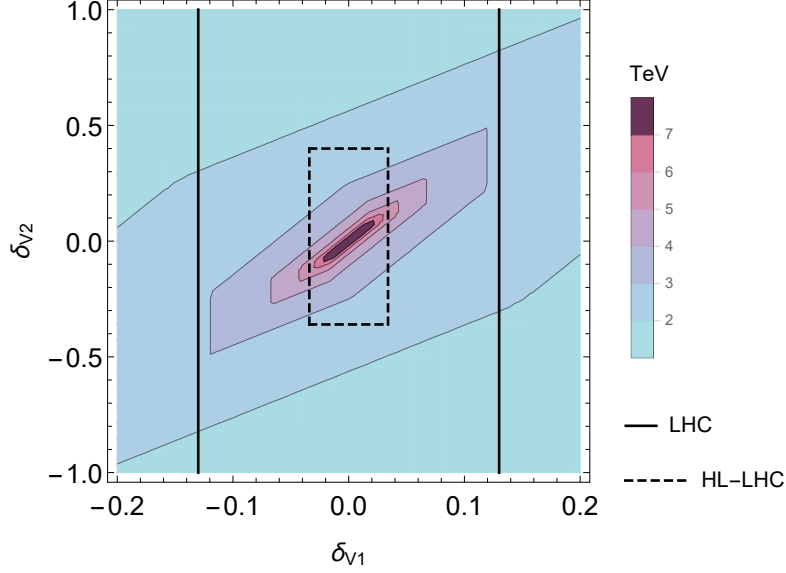


Fig. 12. Unitarity violating contours from δ_{V1} and δ_{V2} . The solid lines represent the ATLAS bound on δ_{V1} [30] while the δ_{V2} bound [35] is outside of the plot range. The dashed lines show the projected bounds for δ_{V1} [24] and δ_{V2} at HL-LHC, where the δ_{V2} bounds are the 95% C.L. bounds from doubling the 68% bounds from a projected vector boson fusion di-Higgs search [34].

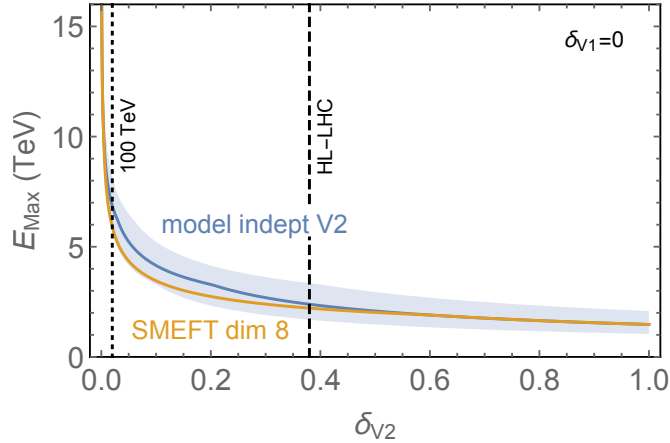


Fig. 13. The unitarity bound from as a function of δ_{V2} neglecting small terms proportional to δ_{V1} . The optimal bound lies between the model-independent and SMEFT estimates. The band around the model-independent bound results from varying the unitarity bound to $\frac{1}{2} \leq |\hat{\mathcal{M}}| \leq 2$. For comparison, we show 95% C.L. limits on the coupling from the vector boson fusion di-Higgs analysis projected for the HL-LHC and a 100 TeV pp collider [34].

the SMEFT unitarity bound as a function of δ_{V2} , neglecting terms proportional to δ_{V1} , showing that the optimal bound is close to the model-independent one.

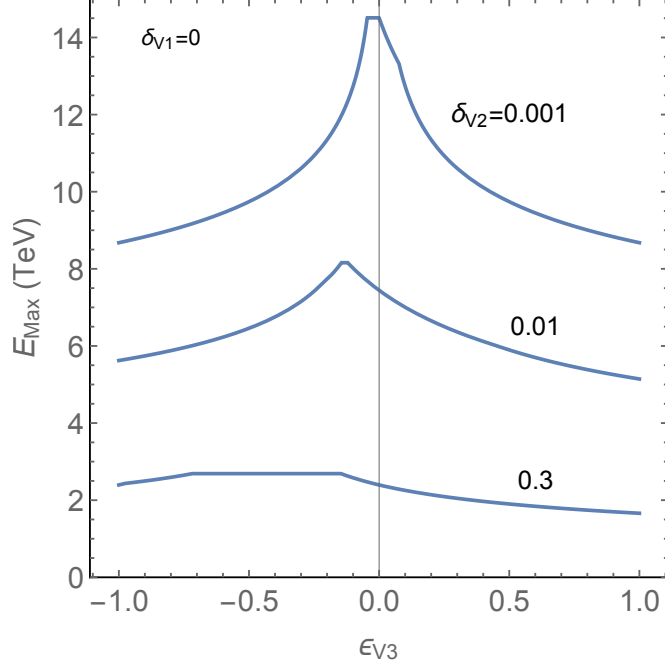


Fig. 14. The unitarity bound from processes that depend on δ_{V2} and $c_{V3} = 8\delta_{V2}(1 + \epsilon_{V3})$ to linear order, where $\epsilon_{V3} = 0$ correspond to the SMEFT predictions, assuming $\delta_{V1} = 0$.

Next, we consider the accuracy of the SMEFT prediction for δ_{V2} from the operator Eq. (5.3). (We again consider the case where $\delta_{V1} = 0$). We expect the predictions of this operator to become more accurate as the scale of new physics becomes large. In Fig. 14 we plot the quantity

$$\epsilon_{V3} = \frac{c_{V3} - c_{V3}^{\text{dim } 8}}{c_{V3}^{\text{dim } 8}}, \quad (5.5)$$

where $c_{V3}^{\text{dim } 8} = 8\delta_{V2}$. As in previous cases, we find that the SMEFT prediction becomes accurate when the scale of new physics is larger than a TeV.

5.3 $hh\bar{t}t$: Model-Independent Bound on the Scale of New Physics

We now consider a deviation in the $hh\bar{t}t$ coupling c_{t2} . The study of this coupling is strongly motivated by the fact that di-Higgs production is sensitive to this coupling, and therefore di-Higgs production does not measure the h^3 coupling in a model-independent way [36]. However, measuring $ht\bar{t}$ and $hht\bar{t}$ production has been shown to break the degeneracies between the hhh , $h\bar{t}t$ and $hh\bar{t}t$ couplings [37–39].

In this subsection we focus on the unitarity bound on c_{t2} . We are interested in model-independent processes that do not depend on c_{tn} for $n \geq 3$. The relevant couplings are given in Eqs. (4.3) and (2.11). We can work out that the model-independent processes have the

schematic form at leading order in the energy expansion:

$$\begin{aligned}
\hat{\mathcal{M}}(\bar{t}t \rightarrow hh) &\sim y_t c_{t2} \frac{E}{v}, \\
\hat{\mathcal{M}}(\bar{t}t \rightarrow V_L hh) &\sim y_t (\delta_{t1} + c_{t2} + \delta_{V1} + \delta_{V2} + \delta_{t1}\delta_{V1} + \delta_{V1}^2) \frac{E^2}{v^2}, \\
\hat{\mathcal{M}}(\bar{t}t \rightarrow V_L V_L h) &\sim y_t (\delta_{t1} + c_{t2} + \delta_{V1} + \delta_{V2} + \delta_{t1}\delta_{V1} + \delta_{t1}\delta_{V2} \\
&\quad + c_{t2}\delta_{V1} + \delta_{V1}^2 + \delta_{t1}\delta_{V1}^2) \frac{E^2}{v^2}, \\
\hat{\mathcal{M}}(\bar{t}t \rightarrow V_L V_L V_L h) &\sim y_t (\delta_{t1} + c_{t2} + \delta_{V1} + \delta_{V2} + \delta_{t1}\delta_{V1} + \delta_{t1}\delta_{V2} \\
&\quad + c_{t2}\delta_{V1} + \delta_{V1}^2 + \delta_{V1}\delta_{V2} + \delta_{t1}\delta_{V1}^2 + \delta_{V1}^3) \frac{E^3}{v^3}, \\
\hat{\mathcal{M}}(\bar{t}t \rightarrow V_L V_L V_L V_L) &\sim y_t (\delta_{t1} + c_{t2} + \delta_{V1} + \delta_{V2} + \delta_{t1}\delta_{V1} + \delta_{t1}\delta_{V2} + c_{t2}\delta_{V1} \\
&\quad + \delta_{V1}^2 + \delta_{V1}\delta_{V2} + \delta_{t1}\delta_{V1}^2 + \delta_{t1}\delta_{V1}\delta_{V2} + c_{t2}\delta_{V1}^2 \\
&\quad + \delta_{V1}^3 + \delta_{V1}^2\delta_{V2} + \delta_{t1}\delta_{V1}^3 + \delta_{V1}^4) \frac{E^4}{v^4}.
\end{aligned} \tag{5.6}$$

For $\bar{t}b$ initial states, the first and third process vanish while the second process does not have a δ_{t1} term. Amplitudes related to these by crossing have the same scaling. Again, due to constraints on δ_{t1}, δ_{V1} we can neglect the nonlinear terms. At linear order, we see that only the $\bar{t}t \rightarrow hh$ amplitude is independent of δ_{V2} , which is poorly constrained experimentally and thus can substantially affect the constraints on c_{t2} . These linear contributions involving δ_{V1} and δ_{V2} involve diagrams with propagators, which are significantly more difficult to compute so we have focused on the terms from δ_{V2} . Due to this contamination from δ_{V2} , we will use only $\bar{t}t \rightarrow hh$ to set unitarity bounds on c_{t2} . The bounds taking into account the dominant linear contributions are:

$$\begin{aligned}
t_R \bar{t}_R \rightarrow hh : \quad E_{\max} &\simeq \frac{7.2 \text{ TeV}}{|c_{t2}|}, \\
t_R \bar{t}_R \rightarrow W_L^+ W_L^- h : \quad E_{\max} &\simeq \frac{4.7 \text{ TeV}}{|c_{t2} - 2\delta_{t1} + \frac{1}{3}\delta_{V2}|^{1/2}}, \\
t_R \bar{b}_R \rightarrow W_L^+ h^2 : \quad E_{\max} &\simeq \frac{4.7 \text{ TeV}}{|c_{t2} - 2\delta_{t1} - \frac{2}{3}\delta_{V2}|^{1/2}}, \\
t_R \bar{b}_R W_L^- \rightarrow h W_L^+ W_L^- : \quad E_{\max} &\simeq \frac{3.9 \text{ TeV}}{|c_{t2} - 3\delta_{t1} + \frac{1}{2}\delta_{V2}|^{1/3}}, \\
t_R \bar{b}_R W_L^- \rightarrow W_L^+ W_L^+ W_L^- W_L^- : \quad E_{\max} &\simeq \frac{4.2 \text{ TeV}}{|c_{t2} - 3\delta_{t1} + \frac{1}{3}\delta_{V2}|^{1/4}}.
\end{aligned} \tag{5.7}$$

In Fig. 15, we plot the unitarity violating scale as a function of c_{t2} and δ_3 . Superimposed on the plot are estimates of the current bounds and sensitivity to these parameters from gluon fusion di-Higgs production [36]. We see that it is plausible that the HL-LHC could

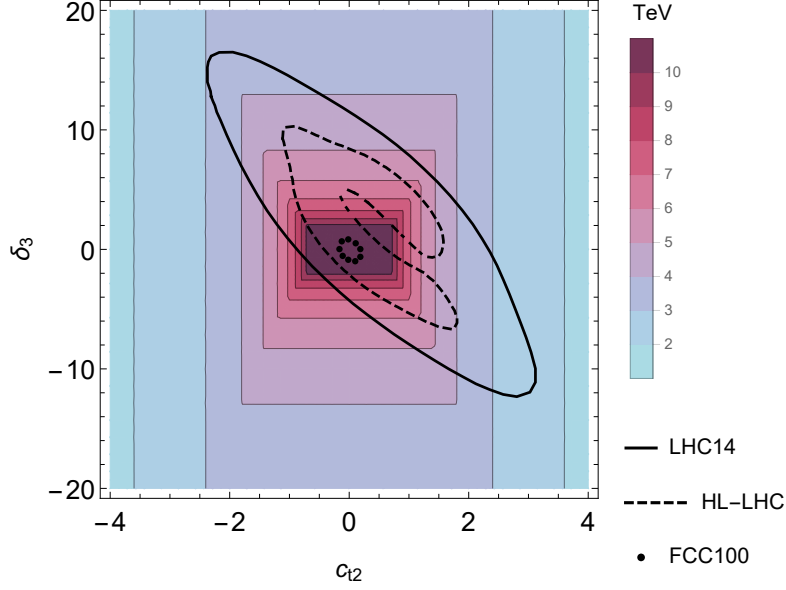


Fig. 15. Unitarity violating contours from δ_3 and c_{t2} . The 95% C.L. projections from gluon fusion di-Higgs searches are shown for the LHC (solid) and for the HL-LHC (dashed), which were obtained by expanding the 1σ contours of [36] by 1.6 to estimate the 95% C.L. sensitivity.

find deviations that point to a scale of new physics below 3 TeV, even allowing for the experimental degeneracy between c_{t2} and δ_3 .

5.4 $hh\bar{t}t$: Optimal Bound and SMEFT Predictions

To obtain the relations between c_{2t} and higher order couplings, we use the dimension-8 SMEFT operator

$$\frac{y_t}{M^4} \left(H^\dagger H - \frac{v^2}{2} \right)^2 (\bar{Q}_L \tilde{H} t_R + \text{h.c.}), \quad (5.8)$$

which gives the predictions

$$\delta_{t1} = 0, \quad c_{t2} = -2 \frac{v^4}{M^4}, \quad c_{t3} = 6c_{t2}, \quad c_{t4} = 15c_{t2}, \quad c_{t5} = 15c_{t2}, \quad (5.9)$$

and $c_{tn} = 0$ for $n \geq 6$. As in the previous cases, we can use Eq. (5.9) to obtain unitarity bounds from processes that we classified as model-independent. Fig 16 shows the unitarity bounds predicted by the model independent approach and the SMEFT operator, where we assume $\delta_{t1} = \delta_{V1} = \delta_{V2} = 0$ to focus on c_{t2} . Thus, the optimal bound is still within our estimated uncertainty of the model-independent bound.

Once again, we can see the effect that a high scale of unitarity violation (compared to 1 TeV) has on the SMEFT predictions in Eq. (5.9). Fig. 17 shows the unitarity scale

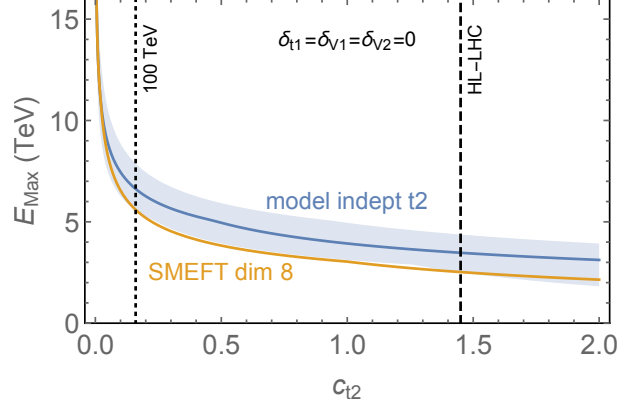


Fig. 16. The unitarity bounds from both the model-independent approach and the SMEFT dimension-8 prediction, the optimized bound from marginalizing over other couplings should be somewhere between these two lines. We assume $\delta_{t1} = \delta_{V1} = \delta_{V2} = 0$. We also plot the projected 95% C.L. limits on the coupling from the gluon fusion di-Higgs analysis at the HL-LHC and a 100 TeV pp collider [36]

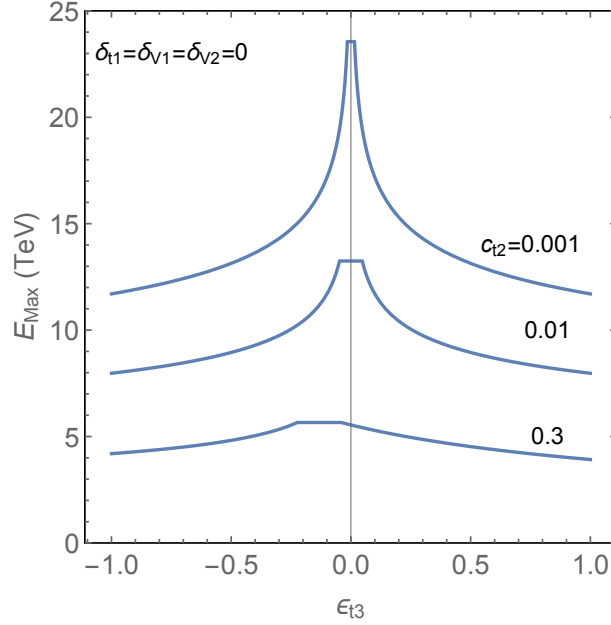


Fig. 17. The unitarity bound from processes that depend only on c_{t2} and $c_{t3} = 6c_{t2}(1 + \epsilon_{t3})$ when $\delta_{t1} = \delta_{V1} = \delta_{V2} = 0$. Setting $\epsilon_{t3} = 0$ corresponds to the SMEFT prediction from the dimension-8 operator.

dependence on ϵ_{t3} where $c_{t3} = 6c_{t2}(1 + \epsilon_{t3})$ and we assume $\delta_{t1} = \delta_{V1} = \delta_{V2} = 0$. As with the other couplings, at high scales of unitarity violation (e.g. 10 TeV), c_{t3} is close to its SMEFT value.

6 Conclusions

In this paper, we have investigated the scale of unitarity violation due to nonstandard Higgs self-couplings, and Higgs couplings to W/Z bosons and top quarks. In the SM, good high energy behavior for multiparticle scattering amplitudes relies on delicate cancellations among the various Higgs couplings. If these cancellations are upset by new physics contributions to the Higgs couplings, this leads to tree-level unitarity violation at high energies, signaling the breakdown of perturbation theory and the onset of new physics. In this way, we can give a model-independent bound on the scale of new physics directly from any observed deviation from the SM prediction for Higgs couplings.

In this work, we focused on the couplings h^3 , h^4 , hVV , h^2VV , $h\bar{t}t$, and $h^2\bar{t}t$ where $V = W$ or Z , which will be probed at the HL-LHC and future colliders. In the SM, these couplings are predicted at the percent level while current constraints are only at the 10%–100% level. Upcoming experiments will significantly improve these constraints, giving many opportunities to discover physics beyond the SM. Our work translates these searches into a direct probe of the scale of new physics.

For the $hVV, h\bar{t}t$ couplings, the current constraints allow coupling values that require new physics below 3 TeV for W/Z couplings, and below 8 TeV for the top coupling. The Higgs trilinear coupling is much more weakly constrained, allowing a scale of new physics as low as 4 TeV. The couplings $hh\bar{t}t$ and $hhVV$ are of particular interest for di-Higgs searches in gluon-fusion and vector boson fusion, and their constraints allow a scale of new physics as low as 2 TeV. These results show that measurements of Higgs couplings can point to a scale of new physics within the kinematic reach for HL-LHC and future colliders.

Unitarity bounds can also place indirect constraints on couplings that are difficult to measure directly, such as the h^4 coupling. For example if there is a nonstandard Higgs trilinear coupling, we show that to keep the new physics bound above 10 TeV, the quartic coupling must closely approximate the coupling correlation from the dimension-6 SMEFT operator $(H^\dagger H)^3$. We present similar results for the W/Z and top couplings as well. We emphasize that these predictions do not make any assumptions about the smallness of higher-dimension operators, and rely only on unitarity.

Our main conclusion is that, from a purely data-driven viewpoint, our current knowledge of the Higgs couplings allows new physics at the few TeV scale. This scale will be extensively probed at the HL-LHC and future colliders, both through direct searches and Higgs coupling measurements, and there is a great deal of room for discovery in both types of analyses. In particular, the scales probed by the upcoming HL-LHC are not sufficiently large that we can confidently neglect higher-dimension operators in SMEFT. We have therefore adopted a completely bottom-up and model-independent approach to translating these measurements into direct statements about the scale of new physics. We hope that these results will be useful in interpreting and further motivating the precision study of the Higgs boson's

properties.

Acknowledgments

We thank T. Cohen, X. Lu, and D. Soper for discussions. The work of SC was supported in part by the U.S. Department of Energy under Grant Number DE-SC0011640. The work of ML and MC was supported in part by the U.S. Department of Energy under grant DE-SC-0009999. The work of FA was supported by the OCEVU Labex (ANR-11-LABX-0060) and the A*MIDEX project (ANR-11-IDEX-0001-02) funded by the “Investissements d’Avenir” French government program, managed by the ANR.

A Calculation Techniques and Results

In this appendix we define the multi-particle amplitudes we use to obtain the unitarity bounds, explain how they are computed, discuss potential infrared enhancements, and give the results of the calculations used in the main text. We extend the results of Ref. [20] to include fermions, momentum-dependent couplings, and tree-level diagrams with propagators.

A.1 Scalar Amplitudes

We first discuss amplitudes involving only scalar fields, which includes amplitudes with longitudinal W and Z bosons when we use the equivalence theorem. Given r species of scalars ϕ_1, \dots, ϕ_r we define the states

$$\begin{aligned} |P; k_1, \dots, k_r\rangle &\equiv C_{k_1, \dots, k_r} \int d^4x e^{-iP \cdot x} \phi_1^{(-)}(x)^{k_1} \dots \phi_r^{(-)}(x)^{k_r} |0\rangle \\ &= C_{k_1, \dots, k_r} \int d\Phi_k(P; p_1, \dots, p_k) |\phi_1(p_1) \dots \phi_r(p_k)\rangle. \end{aligned} \quad (\text{A.1})$$

Here k_1, \dots, k_r are non-negative integers that give the number of each species of particle in the state, $\phi_i^{(-)}$ is the negative frequency (creation operator) part of the interaction picture field ϕ_i , $|\phi_1(p_1) \dots \phi_r(p_k)\rangle$ is an ordinary k -particle state with $k = k_1 + \dots + k_r$, and

$$d\Phi_k(P; p_1, \dots, p_k) = \frac{d^3p_1}{(2\pi)^3} \frac{1}{2E_1} \dots \frac{d^3p_k}{(2\pi)^3} \frac{1}{2E_k} (2\pi)^4 \delta^4(p_1 + \dots + p_k - P) \quad (\text{A.2})$$

is the Lorentz invariant k -body phase space. These states are s -wave states defined by integrating k -particle states over the full phase space. The normalization of the states is chosen to be

$$\langle P'; k' | P; k \rangle = (2\pi)^4 \delta^4(P' - P) \delta_{k'k}, \quad (\text{A.3})$$

where we use the abbreviations

$$|P; k\rangle = |P; k_1, \dots, k_r\rangle, \quad \delta_{k'k} = \delta_{k'_1 k_1} \cdots \delta_{k'_r k_r}, \quad C_k = C_{k_1, \dots, k_r}. \quad (\text{A.4})$$

The normalization constant is given by

$$\frac{1}{|C_k|^2} = k_1! \cdots k_r! \Phi_k(P), \quad (\text{A.5})$$

where

$$\Phi_k(P) = \int d\Phi_k(P) = \frac{1}{8\pi(k-1)!(k-2)!} \left(\frac{E}{4\pi}\right)^{2k-4}, \quad (\text{A.6})$$

is the total volume of phase space for massless particles with center of mass energy $E = \sqrt{P^2}$.

We then consider S -matrix elements between these states:

$$\langle P'; k' | T | P; k \rangle = (2\pi)^4 \delta^4(P' - P) \hat{\mathcal{M}}(P; k_1, \dots, k_r \rightarrow k'_1, \dots, k'_r), \quad (\text{A.7})$$

where $S = 1 + iT$. The amplitude $\hat{\mathcal{M}}$ is Lorentz invariant and depends only on P_μ , so it is a function of E only. With the normalization Eq. (A.3), unitarity of the S matrix implies that these amplitudes satisfy

$$|\hat{\mathcal{M}}| \leq 1. \quad (\text{A.8})$$

For non-forward amplitudes this follows directly from the unitarity of the S -matrix. For forward amplitudes ($k'_i = k_i$) a few additional steps are required to show that this holds for tree-level amplitudes, see Ref. [20]. This is the unitarity constraint we employ in this paper.

The Feynman rules for these amplitudes follow straightforwardly from the standard rules. The result is that the amplitude $\hat{\mathcal{M}}$ are obtained from the standard Lorentz invariant amplitude \mathcal{M} by averaging over the initial and final state phase space:

$$\hat{\mathcal{M}}_{fi}(P) = C_f^* C_i \int d\Phi_f(P) d\Phi_i(P) \mathcal{M}_{fi}, \quad (\text{A.9})$$

where \mathcal{M}_{fi} is the usual Lorentz-invariant amplitude.⁹ Because we are averaging over final state momenta, these amplitudes have contributions from disconnected diagrams, with each disconnected component contributing a $\hat{\mathcal{M}}$ factor, leading to a form $\hat{\mathcal{M}} \propto \Pi_i \hat{\mathcal{M}}_i$. However, the leading contribution to high-energy amplitudes always comes from connected diagrams.

⁹In more detail, Eq. (A.9) is

$$\begin{aligned} \hat{\mathcal{M}}(P; k_1, \dots, k_r \rightarrow k'_1, \dots, k'_r) &= C_{k'}^* C_k \int d\Phi_{k'}(P; p'_1, \dots, p'_{k'}) d\Phi_k(P; p_1, \dots, p_k) \\ &\times \mathcal{M}(\phi_1(p_1) \cdots \phi_r(p_k) \rightarrow \phi_1(p'_1) \cdots \phi_r(p'_{k'})). \end{aligned} \quad (\text{A.10})$$

In simple cases, these amplitudes can be computed in terms of the total volume of phase space given in Eq. (A.6). For example, for a single insertion of a coupling with no derivatives we have

$$\frac{\langle P'; k' | \int d^4x \phi_1^{n_1}(x) \cdots \phi_r^{n_r}(x) | P; k \rangle}{(2\pi)^4 \delta^4(P' - P)} = C_{k'}^* C_k n_1! \cdots n_r! \Phi_{k'}(P) \Phi_k(P) \quad (\text{A.11})$$

$$= \frac{1}{C_{k'} C_k^*} \frac{n_1! \cdots n_r!}{k_1! \cdots k_r! k'_1! \cdots k'_r!}, \quad (\text{A.12})$$

where we assume $n_i = k_i + k'_i$. For diagrams with a single insertion of a vertex containing derivatives, we use the identities

$$\int d\Phi_k(P; p_1, \dots, p_k) p_1^\mu = \frac{P^\mu}{k} \Phi_k(P), \quad (\text{A.13})$$

$$\int d\Phi_k(P; p_1, \dots, p_k) p_1 \cdot p_2 = \frac{P^2}{2 \binom{k}{2}} \Phi_k(P), \quad (\text{A.14})$$

which hold for the case where all particles are massless.

A.2 States with One Fermion

We consider a state containing a single fermion and k scalars

$$\begin{aligned} |P; k_1, \dots, k_r, \alpha, a\rangle &\equiv C'_k \int d^4x e^{-iP \cdot x} \phi_1^{(-)}(x)^{k_1} \cdots \phi_r^{(-)}(x)^{k_r} \psi_{L\alpha}^{a(-)}(x) |0\rangle \\ &= C'_k \int d\Phi_{k+1}(P; p_1, \dots, p_k, q) v_L^\alpha(q) |\phi_1(p_1) \cdots \phi_r(p_k) \bar{\psi}_R^a(q)\rangle, \end{aligned} \quad (\text{A.15})$$

where ψ_L is a left-handed Weyl spinor field, α is a spinor index, and a is a gauge index (*e.g.* a color index). Note that these states are given by phase space integrals of scattering states weighted by a spinor wavefunction, so Eq. (A.9) is modified for amplitudes involving these states. (In the example above, the state created by the left-handed spinor field is a right-handed antifermion.) The normalization of these states is given by

$$\begin{aligned} \langle P'; k, \beta, b | P; k, \alpha, a \rangle &= (2\pi)^4 \delta^4(P' - P) k_1! \cdots k_r! |C'_k|^2 \int d\Phi_{k+1}(P; p_1, \dots, p_k, q) q^\mu \sigma_\mu^{\alpha\dot{\beta}} \delta_{ab} \\ &= (2\pi)^4 \delta^4(P' - P) k_1! \cdots k_r! |C'_k|^2 \delta_{ab} \frac{P \cdot \sigma^{\alpha\dot{\beta}}}{k+1} \Phi_{k+1}, \end{aligned} \quad (\text{A.16})$$

where we used Eq. (A.13). We choose the states Eq. (A.15) to have normalization

$$\langle P'; k', \beta, b | P; k, \alpha, a \rangle = (2\pi)^4 \delta^4(P' - P) \delta_{ab} \delta_{k'k} \frac{P \cdot \sigma^{\alpha\dot{\beta}}}{E}. \quad (\text{A.17})$$

Note that in the P^μ rest frame we have $P \cdot \sigma^{\alpha\dot{\beta}}/E = \delta^{\alpha\dot{\beta}}$, so this is the natural generalization of the normalization condition Eq. (A.3). The normalization constants are therefore given by

$$\frac{1}{|C_k''|^2} = k_1! \cdots k_r! \frac{E}{k+1} \Phi_{k+1}(P). \quad (\text{A.18})$$

A.3 States with Two Fermions

We now consider states with two fermions and k scalars of the form

$$\begin{aligned} |P; k_1, \dots, k_r, L/R\rangle &\equiv C_k'' \int d^4x e^{-iP \cdot x} \phi_1^{(-)}(x)^{k_1} \cdots \phi_r^{(-)}(x)^{k_r} \bar{\psi}_{R/L}^{a(-)}(x) \psi_{L/R}^{a(-)}(x) |0\rangle \\ &= C_k'' \int d\Phi_{k+2}(P; p_1, \dots, p_k, q, q') \bar{u}_{R/L}(q') v_{L/R}(q) \\ &\quad \times \sum_a |\phi_1(p_1) \cdots \phi_r(p_k) \psi_{R/L}^a(q') \bar{\psi}_{R/L}^a(q)\rangle, \end{aligned} \quad (\text{A.19})$$

where ψ_L (ψ_R) are left-handed (right-handed) Weyl spinors. In the massless limit the states $|\dots L\rangle$ and $|\dots R\rangle$ are orthogonal s -wave states, with the L (R) state containing a fermion-antifermion pair which are both right-handed (left-handed) in helicity. These states are normalized as in Eq. (A.3) if we choose

$$\frac{1}{|C_k''|^2} = k_1! \cdots k_r! \frac{2NE^2}{(k+1)(k+2)} \Phi_{k+2}(P), \quad (\text{A.20})$$

where $a = 1, \dots, N$ and for a top quark, $N = N_c$. To compute amplitudes for these states, we use

$$\begin{aligned} &\frac{\langle P'; k' | \int d^4x \phi_1(x)^{n_1} \cdots \phi_r(x)^{n_r} \bar{\psi}_{L/R}(x) \psi_{R/L}(x) | P; k, L/R \rangle}{(2\pi)^4 \delta^4(P' - P)} \\ &= C_{k'}^* C_k'' n_1! \cdots n_r! \frac{2NE^2}{(k+2)(k+1)} \Phi_{k'}(P) \Phi_{k+2}(P), \\ &= \frac{1}{C_{k'}(C_k'')^*} \frac{n_1! \cdots n_r!}{k_1! \cdots k_r! k_1'! \cdots k_r'!}, \end{aligned} \quad (\text{A.21})$$

$$\frac{\langle P'; k' | \int d^4x \phi_1(x)^{n_1} \cdots \phi_r(x)^{n_r} \bar{\psi}_{L/R}(x) \psi_{R/L}(x) | P; k, R/L \rangle}{(2\pi)^4 \delta^4(P' - P)} = 0. \quad (\text{A.22})$$

A.4 Example Calculations

We now give some examples of calculations involving these rules. The amplitudes involving a single insertion of a vertex without derivatives is straightforward using the formulas given

above, and will not be discussed further. Diagrams with derivatives are less trivial because the derivatives may act on fields that are connected with either initial or final state particles. For example, consider

$$\begin{aligned}
\frac{\langle P'; 2 | \int d^4x \phi^2 (\partial\phi)^2 | P; 2 \rangle}{(2\pi)^4 \delta^4(P' - P)} &= \int d^4x \left[\langle P'; 2 | \phi^2 | 0 \rangle \langle 0 | (\partial\phi)^2 | P; 2 \rangle \right. \\
&\quad + \langle P'; 2 | (\partial\phi)^2 | 0 \rangle \langle 0 | \phi^2 | P; 2 \rangle \\
&\quad \left. + 4 \langle P'; 2 | \phi \partial^\mu \phi | 0 \rangle \langle 0 | \phi \partial_\mu \phi | P; 2 \rangle \right] \\
&= 4|C_2|^2 \left(-2 \cdot \frac{1}{2} E^2 + 4 \cdot \frac{-iP^\mu}{2} \frac{iP_\mu}{2} \right) \Phi_2(P)^2 = 0. \tag{A.23}
\end{aligned}$$

The cancellation can be understood at the level of the ordinary amplitude from the fact that crossing symmetry implies that the amplitude is proportional to $s + t + u = 4m_\phi^2$, which vanishes in the massless limit.

We now give an example of a diagram that contains a propagator:

$$\begin{aligned}
&\frac{\langle P'; 0, 0, 2 | \int d^4x (\partial\phi_3)^2 \phi_2 \int d^4y \phi_2 (\partial\phi_1)^2 | P'; 2, 0, 0 \rangle}{(2\pi)^4 \delta^4(P' - P)} \\
&= |C_2|^2 \int d\Phi_2(P'; p'_1, p'_2) d\Phi_2(P; p_1, p_2) (2p'_1 \cdot p'_2) (2p_1 \cdot p_2) \frac{i}{P^2} \\
&= |C_2|^2 \frac{i}{E^2} [E^2 \Phi_2(P)]^2. \tag{A.24}
\end{aligned}$$

Diagrams with propagators are generally subleading at high energies compared to diagrams with a single insertion. There are a few relevant exceptions, which are discussed in the main paper.

A.5 IR Enhancement

The amplitudes $\hat{\mathcal{M}}$ are dimensionless, and once coupling constants have been factored out, they depend on a single dimensionful variable E in the massless limit. The dependence on E is therefore determined by dimensional analysis, provided that there are no IR enhancements in the massless limit. Such IR enhancements can arise because the integration over initial and final state phase space can go over regions where internal propagators go on shell. We now present arguments that such IR enhancements do not invalidate the leading large E scaling for any of the processes used to set the unitarity bounds in this paper. First, we show that many (but not all) possible IR enhancements can be ruled out by a simple parametric argument. Second, we give a diagrammatic argument that IR enhancements can modify the naïve power counting by at most corrections of order $\log(E/m)^n$ for some positive integer n , where m is the mass of a SM particle such as m_W or m_h . Finally, we point out that the

gauge boson equivalence theorem itself is invalid in the phase space region of the potential IR enhancements, since these are regions where some Lorentz invariants $p_i \cdot p_j \sim m_W^2$ rather than E^2 . Therefore, phase space integration over these regions is suspect. (We note that this issue arises already for $2 \rightarrow 2$ partial wave amplitudes.) We argue that, because the singular phase space regions are parametrically small, they cannot give rise to additional $\log(E/m_W)$ enhancements, and therefore the Goldstone amplitudes correctly give the correct leading behavior at large E .

For the parametric argument, consider an amplitude with leading large- E behavior

$$\hat{\mathcal{M}} \sim C \left(\frac{E}{v} \right)^n \left(\frac{E}{m} \right)^r \log(E/m)^s, \quad (\text{A.25})$$

where C is a BSM coupling, m is an IR mass (such as m_W or m_h), and n, r, s are non-negative integers. Observe that if $r + s > 0$ this becomes arbitrarily large for any fixed E in the limit $m \rightarrow 0$ with v and c fixed. But the amplitude cannot become arbitrarily large in this limit because the massless limit is equivalent to a weak-coupling limit where the SM couplings $g, \lambda, y_t \rightarrow 0$. The coupling C is held fixed in this limit, but can be chosen to be arbitrarily small. It is clear that we cannot have unitarity violation at arbitrary energy scales in this limit, so IR enhancements of the form Eq. (A.25) are ruled out.

Note that the combinations $\lambda\delta_3$, $\lambda\delta_4$, λc_n , $y_t\delta_{t1}$, and $y_t c_{tn}$ should be viewed as BSM couplings that are held fixed in the limit $\lambda, y_t \rightarrow 0$. On the other hand, the couplings δ_{V1} , δ_{V2} , and c_{Vn} for $n \geq 3$ should be held fixed in the $g \rightarrow 0$ limit, since these give Nambu-Goldstone interactions of finite strength in this limit. This limit rules out many possible IR enhancements, but it is not sufficient to justify the power counting of the amplitudes in Eqs. (2.5), (3.8), (4.5), (5.1), and (5.6). In particular, it does not rule out power IR enhancements proportional to additional powers of the SM couplings g, λ, y_t , for example

$$\lambda \frac{E^2}{m_h^2} \sim \frac{E^2}{v^2}, \quad y_t \frac{E}{m_t} \sim \frac{E}{v}, \quad g^2 \frac{E^2}{m_W^2} \sim \frac{E^2}{v^2}, \quad (\text{A.26})$$

which have a finite weak-coupling limit as well as log terms such as

$$\lambda \ln(E^2/m_h^2), \quad y_t \ln(E/m_t), \quad g^2 \ln(E^2/m_W^2), \quad (\text{A.27})$$

which go to zero as $\lambda, y_t, g \rightarrow 0$.

Next, by examining the structure of the exchange diagrams, we will now argue that the IR enhancement of tree diagrams is at most logarithmic. In all the amplitudes we computed, we find that such logs are absent, although they may well be present in more complicated diagrams that we have not computed. As we point out below, even though the equivalence theorem cannot be trusted in parts of the phase space where the IR enhancement occurs, it is valid for a parametrically large region that could contribute to a logarithmic enhancement. Therefore, the absence of logs in our calculations prove that the corresponding longitudinal

gauge boson scattering amplitudes are free of logs. By excising the small untrustworthy regions, we will then argue that the Nambu-Goldstone amplitudes can be used to set a conservative limit on the unitarity violating scale. A better theoretical understanding of these log corrections is desirable, but we will leave this for future work.

We now consider possible IR enhancements from a general tree diagram contributing to the integrated amplitude $\hat{\mathcal{M}}$, whether computed in the full SM or using the equivalence theorem. An IR divergence can arise only from integrating over a region where an internal propagator becomes large. This can happen if the momentum flowing through an internal line goes on shell, or is soft. If only a single propagator goes on shell, it is easy to understand why the correction is at most logarithmic. Consider an internal line with momentum $q - q'$, where q (q') is the momentum of one of the initial (final) state particles. Then the relevant part of the phase space integral is (in the massless limit)

$$d^4q \delta(q^2) d^4q' \delta(q'^2) \frac{1}{(q - q')^2} \propto \frac{d|\vec{q}| d|\vec{q}'| d\cos\theta}{1 - \cos\theta}, \quad (\text{A.28})$$

where θ is the angle between \vec{q} and \vec{q}' . This integral diverges at most logarithmically because the integral has a simple pole in $\cos\theta$, which is one of the integration variables. A general propagator with more legs attached can be analyzed by considering the following momenta structure $P_1 + P_2 \rightarrow K_1 + K_2$ where $P_1 = (p_1 + \dots + p_r)$, $P_2 = (p_{r+1} + \dots + p_n)$, $K_1 = (k_1 + \dots + k_s)$, $K_2 = (k_{s+1} + \dots + k_m)$ and the momentum flowing through the propagator is $K_1 - P_1$. By factorizing the incoming n -body phase into $r + (n - r)$ -body phase space and similarly for the outgoing, we also see this propagator gives a log when integrating over $\cos\theta = \vec{P}_1 \cdot \vec{K}_1 / (|\vec{P}_1| |\vec{K}_1|)$.

Next, we have to consider regions of the phase space integration where more than one propagator gets large at the same time. In all the cases we studied, the denominator of each of the large propagators has a linear zero that depends on an independent parameter, either another angle or invariant mass of a set of particles, that is integrated over. That is, near the singularity the integral behaves like $\int dx dy / xy$ and not $\int dx / x^2$. We checked this for $2 \rightarrow 2$ and $2 \rightarrow 3$ topologies, but we do not have a general proof for all topologies. However, this makes intuitive sense given that a set of n internal propagators going onshell requires n independent conditions on the phase space. Integrating over each of these conditions, then gives at most a $\log^n(E/m)$ singularity.¹⁰

We now note that in cases where there is a log enhancement in an amplitude involving longitudinal gauge bosons, it is not obvious whether the corresponding Nambu-Goldstone amplitude correctly reproduces these logs. The gauge boson equivalence theorem guarantees that the Nambu-Goldstone amplitude correctly reproduces the full amplitude if $|p_i \cdot p_j| \gg m_V^2$ for all external 4-momenta p_i and more generally for all Mandelstam invariants. To see this,

¹⁰In Ref. [2] it is stated without proof that the $2 \rightarrow n$ partial wave amplitudes have at most logarithmic singularities.

compare the exact dot products of longitudinal polarization vectors

$$\epsilon_L(p_1) \cdot \epsilon_L(p_2) = \frac{E_1 E_2}{m_V^2} \left(\frac{|\vec{p}_1| |\vec{p}_2|}{E_1 E_2} - \cos \theta \right) \quad (\text{A.29})$$

with the approximation $\epsilon_L^\mu(p) \simeq p^\mu/m_V$:

$$\frac{p_1}{m_V} \cdot \frac{p_2}{m_V} = \frac{E_1 E_2}{m_V^2} \left(1 - \frac{|\vec{p}_1| |\vec{p}_2|}{E_1 E_2} \cos \theta \right), \quad (\text{A.30})$$

where θ is the angle between \vec{p}_1 and \vec{p}_2 . For $E_{1,2} \gg m_V^2$ and $\cos \theta \ll 1$, these are equal up to corrections suppressed by m_V^2/E^2 . But for $\theta \sim m_V/E$, the dot products are completely different. (For $\theta = 0$, they even have opposite sign.) This means that we cannot expect the equivalence theorem to be correct in regions where some of the Mandelstam invariants are small.

This is relevant for the present discussion because these regions are precisely the ones where one or more internal propagators can go on shell in the massless limit, potentially giving an IR enhancement. However, we note that the regions where the gauge boson equivalence theorem does not apply are a parametrically small part of the phase space integral. Integrals over such regions cannot give rise to IR singularities of the form $\log(E/m)$, which instead arise from integrals of the form $\sim \int dx/x$ over a parametrically large range $\Delta x \sim E/m$. Thus, for example, when we obtain a Goldstone amplitude \hat{M} that does not have a $\log(E/m)$ enhancement, we know that the corresponding gauge boson amplitude also does not have such an IR enhancement. Omitting the singular region from the phase space integral in a Goldstone amplitude without a log IR enhancement only changes the answer by a small correction suppressed by powers of m_W/E , and therefore gives a good approximation to the exact amplitude.

The discussion above has been less systematic than we would like. It would be nice to have a better understanding of the gauge boson equivalence theorem for partial wave amplitudes, including the IR enhancements and subleading contributions. We leave this for future work.

A.6 Results

We now give the results for the leading high-energy behavior for the processes used in the main text in tables 1-10. All gauge bosons are understood to be longitudinally polarized. Also, note that since Z_L is CP-odd, amplitudes involving an odd number of Z_L 's will be purely imaginary, however, these amplitudes can be made real by redefining the Z_L states. All other processes are related to the ones listed in the tables via charge conjugation and/or crossing symmetry. All of these amplitudes are calculated in the contact approximation. As Eqs. (3.8), (4.5), (5.1), and (5.6) show, the nonlinear terms are small due to constraints on δ_{V1}, δ_{t1} . However, there are linear terms proportional to δ_{V1}, δ_{V2} in the top processes Eqs. (4.5) and (5.6), so we've calculated the largest terms as shown in Eqs. (4.1) and (5.7).

Process	$\times \frac{\delta_{V1} E^2}{8\pi v^2}$	Process	$\times \frac{(\delta_{V1} - \frac{1}{2}\delta_{V2}) E^2}{8\pi v^2}$
$ZZ \rightarrow W^+ W^-$	$-\sqrt{2}$	$hZ \rightarrow hZ$	-1
$W^+ W^+ \rightarrow W^+ W^+$	1	$ZZ \rightarrow hh$	1
$ZW^+ \rightarrow ZW^+$	1	$hW^+ \rightarrow hW^+$	-1
$W^+ W^- \rightarrow W^+ W^-$	-1	$hh \rightarrow W^+ W^-$	$\sqrt{2}$

Table 1. 4-body model-independent unitarity-violating process from modifications to the Higgs coupling to W/Z bosons. The left-hand side amplitudes are model-independent since they only depend on δ_{V1} while the ones on right-hand side depend on δ_{V2} as well.

Process	$\times \frac{(\delta_{V2} - 4\delta_{V1}) E^3}{96\pi^2 v^3}$	Process	$\times \frac{(\delta_{V2} - 4\delta_{V1}) E^3}{96\pi^2 v^3}$
$hW^+ W^+ \rightarrow W^+ W^+$	$\sqrt{2}$	$hW^- W^+ \rightarrow ZZ$	-2
$hW^+ W^- \rightarrow W^+ W^-$	$-\sqrt{2}$	$ZW^- W^+ \rightarrow hZ$	0
$W^- W^+ W^+ \rightarrow hW^+$	0	$Z^3 \rightarrow hZ$	0
$ZZW^+ \rightarrow hW^+$	0	$Z^2 h \rightarrow Z^2$	0
$hZW^+ \rightarrow ZW^+$	$\sqrt{2}$	$Z^2 h \rightarrow W^+ W^-$	-2

Table 2. 5-body unitarity-violating processes that depend on δ_{V2} and δ_{V1} . One can see that the dim-6 SMEFT prediction $\delta_{V2} = 4\delta_{V1}$ gives vanishing amplitudes for all processes.

Process	$\times \frac{\delta_{Z1} E^2}{8\pi v^2}$	Process	$\times \frac{\delta_{Z1} E^3}{24\pi^2 v^3}$
$ZZ \rightarrow ZZ$	0	$W^+ W^- \rightarrow Z^3$	0
$ZZ \rightarrow W^+ W^-$	$-\frac{1}{\sqrt{2}}(1 + \lambda_{WZ})$	$ZW^+ \rightarrow Z^2 W^+$	0
$ZW^+ \rightarrow ZW^+$	$\frac{1}{2}(1 + \lambda_{WZ})$	$Z^2 \rightarrow ZW^+ W^-$	0
$W^+ W^- \rightarrow W^+ W^-$	$-\lambda_{WZ}$	$W^+ W^- \rightarrow ZW^+ W^-$	0
$W^+ W^+ \rightarrow W^+ W^+$	λ_{WZ}	$W^+ W^+ \rightarrow ZW^+ W^+$	0
$hW^+ \rightarrow ZW^+$	$\frac{3i}{2}(1 - \lambda_{WZ})$	$ZW^+ \rightarrow W^+ W^- W^+$	$i(1 - \lambda_{WZ})$
$W^+ W^- \rightarrow hZ$	0		

Table 3. 4-body and some 5-body unitarity-violating processes without assuming custodial symmetry. Here $\lambda_{WZ} = \frac{\delta_{W1}}{\delta_{Z1}} = 1$ in the custodial-preserving limit.

Process	$\times \frac{(\delta_{V2}-4\delta_{V1})E^4}{384\pi^3v^4}$
$ZZZ \rightarrow ZZZ$	0
$W^+W^+W^+ \rightarrow W^+W^+W^+$	1
$ZW^+W^+ \rightarrow ZW^+W^+$	1
$ZW^+W^- \rightarrow ZZZ$	$-\sqrt{\frac{2}{3}}$
$ZZW^+ \rightarrow W^+W^+W^-$	$-\frac{2}{3}$
$ZZW^+ \rightarrow ZZW^+$	$\frac{2}{3}$
$ZW^+W^- \rightarrow ZW^+W^-$	$\frac{1}{3}$
$W^+W^+W^- \rightarrow W^+W^+W^-$	$-\frac{1}{3}$

Table 4. 6-body unitarity-violating processes that depend on δ_{V2} and δ_{V1} . One can see that the dim-6 SMEFT prediction $\delta_{V2} = 4\delta_{V1}$ gives vanishing amplitudes for all processes.

Process	$\times \frac{E^4}{1152\pi^3v^4}$
$hZ^2 \rightarrow hZ^2$	$[4\delta_{V1} - 2\delta_{V2} + \frac{1}{2}c_{V3}]$
$h^2Z \rightarrow Z^3$	$-\frac{\sqrt{3}}{2}[4\delta_{V1} - 2\delta_{V2} + \frac{1}{2}c_{V3}]$
$h^2W^+ \rightarrow Z^2W^+$	$-\frac{1}{2}[4\delta_{V1} - 2\delta_{V2} + \frac{1}{2}c_{V3}]$
$h^2Z \rightarrow ZW^+W^-$	$-\frac{1}{\sqrt{2}}[4\delta_{V1} - 2\delta_{V2} + \frac{1}{2}c_{V3}]$
$h^2W^+ \rightarrow W^+W^-W^+$	$-[4\delta_{V1} - 2\delta_{V2} + \frac{1}{2}c_{V3}]$
$hZW^+ \rightarrow hZW^+$	$[36\delta_{V1} - 13\delta_{V2} + 2c_{V3}]$
$hW^+W^+ \rightarrow hW^+W^+$	$[36\delta_{V1} - 13\delta_{V2} + 2c_{V3}]$
$hW^+W^- \rightarrow hW^+W^-$	$-[28\delta_{V1} - 9\delta_{V2} + c_{V3}]$
$hZ^2 \rightarrow hW^+W^-$	$-\sqrt{2}[32\delta_{V1} - 11\delta_{V2} + \frac{3}{2}c_{V3}]$

Table 5. 6-body unitarity-violating processes that depend on δ_{V1} , δ_{V2} , and c_{V3} . One can see that the dim-6 SMEFT prediction $\delta_{V2} = 4\delta_{V1}$ and $c_{V3} = 8\delta_{V1}$ gives vanishing amplitudes for all processes.

Process	$\times \frac{m_t \delta_{t1} E}{8\pi v^2}$	Process	$\times \frac{m_t \delta_{t1} E}{8\pi v^2}$
$\bar{t}_R t_R \rightarrow Zh$	$i\sqrt{N_c}$	$t_R W^+ \rightarrow t_L W^+$	$-\frac{1}{2}$
$\bar{t}_R t_R \rightarrow ZZ$	$-\sqrt{\frac{N_c}{2}}$	$\bar{b}_R t_R \rightarrow hW^+$	$\sqrt{2N_c}$
$\bar{t}_R t_R \rightarrow W^- W^+$	$-\sqrt{N_c}$	$t_R h \rightarrow b_L W^+$	$\frac{1}{\sqrt{2}}$
$t_R Z \rightarrow t_L h$	$\frac{i}{2}$	$t_R W^- \rightarrow b_L h$	$\frac{1}{\sqrt{2}}$
$t_R Z \rightarrow t_L Z$	$-\frac{1}{2}$		
Process	$\times \frac{m_t c_{t2} E}{8\pi v^2}$	Process	$\times \frac{m_t c_{t2} E}{8\pi v^2}$
$\bar{t}_R t_R \rightarrow hh$	$-\sqrt{\frac{N_c}{2}}$	$t_R h \rightarrow t_L h$	$-\frac{1}{2}$

Table 6. 4-body model-independent unitarity-violating processes from the top sector.

Process	$\times \frac{m_t \delta_{t1} E^2}{64\pi^2 v^3}$	Process	$\times \frac{m_t \delta_{t1} E^2}{64\pi^2 v^3}$
$\bar{t}_R t_R \rightarrow ZZZ$	$i\sqrt{3N_c}$	$Z^2 \rightarrow \bar{t}_L b_L W^+$	$\sqrt{\frac{2N_c}{3}}$
$\bar{t}_R t_R \rightarrow ZW^+ W^-$	$i\sqrt{2N_c}$	$ZW^- \rightarrow Zb_L \bar{t}_L$	$2\sqrt{\frac{N_c}{3}}$
$t_R Z \rightarrow t_L W^- W^+$	$\frac{i}{\sqrt{3}}$	$t_R Z \rightarrow b_L ZW^+$	$\sqrt{\frac{2}{3}}$
$t_R Z \rightarrow t_L ZZ$	$i\sqrt{\frac{3}{2}}$	$t_R W^- \rightarrow b_L Z^2$	$\frac{1}{\sqrt{3}}$
$t_R W^+ \rightarrow t_L ZW^+$	$\frac{i}{\sqrt{3}}$	$\bar{b}_R t_R \rightarrow W^+ W^+ W^-$	$2\sqrt{2N_c}$
$W^+ W^- \rightarrow \bar{t}_L t_L Z$	$i\sqrt{\frac{2N_c}{3}}$	$W^- W^- \rightarrow b_L \bar{t}_L W^-$	$2\sqrt{\frac{2N_c}{3}}$
$W^+ Z \rightarrow \bar{t}_L t_L W^+$	$i\sqrt{\frac{2N_c}{3}}$	$W^+ W^- \rightarrow b_L \bar{t}_L W^+$	$4\sqrt{\frac{N_c}{3}}$
$ZZ \rightarrow \bar{t}_L t_L Z$	$i\sqrt{3N_c}$	$t_R W^+ \rightarrow b_L W^+ W^+$	$2\sqrt{\frac{N_c}{3}}$
$\bar{b}_R t_R \rightarrow Z^2 W^+$	$\sqrt{2N_c}$	$t_R W^- \rightarrow b_L W^- W^+$	$2\sqrt{\frac{2N_c}{3}}$

Table 7. 5-body model-independent unitarity-violating processes from the top sector.

Process	$\times \frac{(\frac{1}{2}c_{t2}-\delta_{t1})m_t E^2}{32\pi^2 v^3}$	Process	$\times \frac{(\frac{1}{2}c_{t2}-\delta_{t1})m_t E^2}{32\pi^2 v^3}$
$\bar{t}_R t_R \rightarrow Zh^2$	$i\sqrt{N_c}$	$\bar{t}_R t_R \rightarrow W^+ W^- h$	$-\sqrt{2N_c}$
$h^2 \rightarrow Z\bar{t}_L t_L$	$i\sqrt{\frac{N_c}{3}}$	$W^+ W^- \rightarrow \bar{t}_L t_L h$	$-\sqrt{\frac{2N_c}{3}}$
$Zh \rightarrow h\bar{t}_L t_L$	$i\sqrt{\frac{2N_c}{3}}$	$W^+ h \rightarrow \bar{t}_L t_L W^+$	$-\sqrt{\frac{2N_c}{3}}$
$t_R Z \rightarrow t_L h^2$	$\frac{i}{\sqrt{6}}$	$t_R W^+ \rightarrow t_L W^+ h$	$-\frac{1}{\sqrt{3}}$
$t_R h \rightarrow t_L Zh$	$\frac{i}{\sqrt{3}}$	$t_R h \rightarrow t_L W^+ W^-$	$-\frac{1}{\sqrt{3}}$
$\bar{t}_R t_R \rightarrow Z^2 h$	$-\sqrt{N_c}$	$\bar{b}_R t_R \rightarrow W^+ h^2$	$\sqrt{2N_c}$
$Z^2 \rightarrow \bar{t}_L t_L h$	$-\sqrt{\frac{N_c}{3}}$	$W^- h \rightarrow b_L \bar{t}_L h$	$2\sqrt{\frac{N_c}{3}}$
$Zh \rightarrow \bar{t}_L t_L Z$	$-\sqrt{\frac{2N_c}{3}}$	$h^2 \rightarrow b_L \bar{t}_L W^+$	$\sqrt{\frac{2N_c}{3}}$
$t_R h \rightarrow t_L Z^2$	$-\frac{1}{\sqrt{6}}$	$t_R W^- \rightarrow b_L h^2$	$\frac{1}{\sqrt{3}}$
$t_R Z \rightarrow t_L Zh$	$-\frac{1}{\sqrt{3}}$	$t_R h \rightarrow b_L W^+ h$	$\sqrt{\frac{2}{3}}$

Table 8. 5-body unitarity-violating processes that depend on c_{t2} and δ_{t1} .

Process	$\times \frac{(3\delta_{t1}-c_{t2})m_t E^3}{256\pi^3 v^4}$	Process	$\times \frac{(3\delta_{t1}-c_{t2})m_t E^3}{256\pi^3 v^4}$
$\bar{t}_R t_R Z \rightarrow Z^3$	$\sqrt{\frac{N_c}{2}}$	$t_R Z^2 \rightarrow t_L Z h$	$-\frac{i}{\sqrt{2}}$
$t_R Z^2 \rightarrow t_L Z^2$	$\frac{1}{2}$	$\bar{t}_R t_R Z \rightarrow h W^+ W^-$	$-i\sqrt{\frac{N_c}{3}}$
$\bar{t}_R t_R W^+ \rightarrow Z^2 W^+$	$\sqrt{\frac{N_c}{6}}$	$t_R Z h \rightarrow t_L W^+ W^-$	$-\frac{i}{3}$
$\bar{t}_R t_R Z \rightarrow Z W^+ W^-$	$\sqrt{\frac{N_c}{3}}$	$\bar{b}_R t_R W^- \rightarrow h Z^2$	$-\sqrt{\frac{N_c}{3}}$
$t_R Z^2 \rightarrow t_L W^+ W^-$	$\frac{1}{3\sqrt{2}}$	$\bar{b}_R t_R Z \rightarrow h Z W^+$	$-\sqrt{\frac{2N_c}{3}}$
$t_R Z W^+ \rightarrow t_L Z W^+$	$\frac{1}{3}$	$t_R Z^2 \rightarrow b_L W^+ h$	$-\frac{1}{3}$
$\bar{t}_R t_R W^+ \rightarrow W^+ W^+ W^-$	$\sqrt{\frac{2N_c}{3}}$	$t_R Z h \rightarrow b_L Z W^+$	$-\frac{\sqrt{2}}{3}$
$t_R W^+ W^+ \rightarrow t_L W^+ W^+$	$\frac{1}{3}$	$\bar{b}_R t_R h \rightarrow W^+ W^+ W^-$	$-2\sqrt{\frac{N_c}{3}}$
$t_R W^+ W^- \rightarrow t_L W^+ W^-$	$\frac{2}{3}$	$\bar{b}_R t_R W^- \rightarrow h W^+ W^-$	$-2\sqrt{\frac{2N_c}{3}}$
$\bar{t}_R t_R h \rightarrow Z^3$	$-i\sqrt{\frac{N_c}{2}}$	$t_R W^- W^- \rightarrow b_L W^- h$	$-\frac{2}{3}$
$\bar{t}_R t_R Z \rightarrow Z^2 h$	$-i\sqrt{\frac{3N_c}{2}}$	$t_R W^- h \rightarrow b_L W^+ W^-$	$-\frac{2\sqrt{2}}{3}$
$\bar{b}_R t_R W^+ \rightarrow h W^+ W^+$	$-2\sqrt{\frac{N_c}{3}}$		

Table 9. 6-body unitarity-violating processes that depend on c_{t2} and δ_{t1} . One can see that the dim-6 SMEFT prediction $c_{t2} = 3\delta_{t1}$ gives vanishing amplitudes for all processes.

Process	$\times \frac{(c_{t2}-3\delta_{t1})m_t E^4}{1024\pi^4 v^5}$	Process	$\times \frac{(c_{t2}-3\delta_{t1})m_t E^4}{1024\pi^4 v^5}$
$\bar{t}_R t_R Z \rightarrow Z^4$	$\frac{5i}{4} \sqrt{\frac{N_c}{3}}$	$ZW^+W^+ \rightarrow \bar{t}_L t_L W^+W^+$	$\frac{i\sqrt{N_c}}{6}$
$\bar{t}_R t_R W^+ \rightarrow W^+Z^3$	$\frac{i}{2} \sqrt{\frac{N_c}{3}}$	$ZW^+W^- \rightarrow \bar{t}_L t_L Z^2$	$\frac{i}{2} \sqrt{\frac{N_c}{2}}$
$\bar{t}_R t_R W^+ \rightarrow ZW^-W^+W^+$	$\frac{i\sqrt{N_c}}{3}$	$ZW^+W^- \rightarrow \bar{t}_L t_L W^+W^-$	$\frac{i\sqrt{N_c}}{3}$
$\bar{t}_R t_R Z \rightarrow W^+W^+W^-W^-$	$\frac{i}{3} \sqrt{\frac{N_c}{2}}$	$W^+W^+W^- \rightarrow \bar{t}_L t_L ZW^+$	$\frac{i}{3} \sqrt{\frac{N_c}{2}}$
$t_R Z^2 \rightarrow t_L ZW^-W^+$	$\frac{i}{4}$	$\bar{b}_R t_R W^- \rightarrow Z^4$	$\frac{1}{4} \sqrt{\frac{2N_c}{3}}$
$t_R Z^2 \rightarrow t_L Z^3$	$\frac{5i}{4\sqrt{6}}$	$\bar{b}_R t_R Z \rightarrow W^+Z^3$	$\frac{1}{2} \sqrt{\frac{2N_c}{3}}$
$t_R W^+W^+ \rightarrow t_L ZW^+W^+$	$\frac{i}{6\sqrt{2}}$	$Z^3 \rightarrow b_L \bar{t}_L ZW^+$	$\frac{1}{2} \sqrt{\frac{N_c}{3}}$
$t_R W^-W^+ \rightarrow t_L Z^3$	$\frac{i}{4\sqrt{3}}$	$Z^2W^- \rightarrow b_L \bar{t}_L Z^2$	$\frac{1}{2} \sqrt{\frac{N_c}{2}}$
$t_R W^-W^+ \rightarrow t_L ZW^+W^-$	$\frac{i}{3\sqrt{2}}$	$t_R Z^2 \rightarrow b_L W^+Z^2$	$\frac{1}{4}$
$t_R ZW^+ \rightarrow t_L Z^2W^+$	$\frac{i}{4}$	$t_R ZW^- \rightarrow b_L Z^3$	$\frac{\sqrt{2}}{4\sqrt{3}}$
$t_R ZW^+ \rightarrow t_L W^+W^+W^-$	$\frac{i}{6}$	$\bar{b}_R t_R W^+ \rightarrow W^+W^+Z^2$	$\frac{\sqrt{N_c}}{3}$
$Z^3 \rightarrow \bar{t}_L t_L Z^2$	$\frac{5i}{4} \sqrt{\frac{N_c}{3}}$	$\bar{b}_R t_R W^- \rightarrow Z^2W^+W^-$	$\frac{\sqrt{2N_c}}{3}$
$Z^3 \rightarrow \bar{t}_L t_L W^+W^-$	$\frac{i}{2} \sqrt{\frac{N_c}{6}}$	$W^+W^-W^- \rightarrow b_L \bar{t}_L Z^2$	$\frac{1}{3} \sqrt{\frac{N_c}{2}}$
$Z^2W^+ \rightarrow \bar{t}_L t_L ZW^+$	$\frac{i}{2} \sqrt{\frac{N_c}{2}}$	$ZW^-W^- \rightarrow b_L \bar{t}_L ZW^-$	$\frac{\sqrt{N_c}}{3}$
$t_R W^-W^- \rightarrow b_L W^-Z^2$	$\frac{1}{6}$	$W^+W^-W^- \rightarrow b_L \bar{t}_L W^-W^+$	$\sqrt{N_c}$
$t_R W^+W^- \rightarrow b_L Z^2W^+$	$\frac{\sqrt{2}}{6}$	$W^+W^+W^- \rightarrow b_L \bar{t}_L W^+W^+$	$\sqrt{\frac{N_c}{2}}$
$t_R ZW^- \rightarrow b_L ZW^-W^+$	$\frac{1}{3}$	$t_R W^+W^+ \rightarrow b_L W^+W^+W^+$	$\frac{1}{2\sqrt{3}}$
$\bar{b}_R t_R W^+ \rightarrow W^+W^+W^+W^-$	$\sqrt{\frac{2N_c}{3}}$	$t_R W^-W^- \rightarrow b_L W^+W^-W^-$	$\frac{1}{2}$
$\bar{b}_R t_R W^- \rightarrow W^-W^-W^+W^+$	$\sqrt{N_c}$	$t_R W^+W^- \rightarrow b_L W^-W^+W^+$	$\frac{1}{\sqrt{2}}$
$W^-W^-W^- \rightarrow b_L \bar{t}_L W^-W^-$	$\sqrt{\frac{N_c}{6}}$	$t_R Z^2 \rightarrow b_R W^+W^-W^+$	$\frac{1}{6}$
$\bar{t}_R t_R Z \rightarrow W^+W^-Z^2$	$\frac{i\sqrt{N_c}}{2}$	$\bar{b}_R t_R ZW^- \rightarrow W^+W^-Z$	$\frac{\sqrt{2N_c}}{3}$
$\bar{b}_R t_R W^+W^- \rightarrow Z^2W^+$	$\frac{\sqrt{N_c}}{3}$	$\bar{b}_R t_R Z \rightarrow W^+W^-W^+Z$	$\frac{\sqrt{2N_c}}{3}$

Table 10. 7-body unitarity-violating processes that depend on c_{t2} and δ_{t1} . One can see that the dim-6 SMEFT prediction $c_{t2} = 3\delta_{t1}$ gives vanishing amplitudes for all processes.

References

- [1] C. Llewellyn Smith, “High-Energy Behavior and Gauge Symmetry,” *Phys. Lett. B* **46** (1973) 233–236.
- [2] J. M. Cornwall, D. N. Levin, and G. Tiktopoulos, “Uniqueness of spontaneously broken gauge theories,” *Phys. Rev. Lett.* **30** (1973) 1268–1270. [Erratum: *Phys.Rev.Lett.* 31, 572 (1973)].
- [3] S. D. Joglekar, “S matrix derivation of the Weinberg model,” *Annals Phys.* **83** (1974) 427.
- [4] J. M. Cornwall, D. N. Levin, and G. Tiktopoulos, “Derivation of Gauge Invariance from High-Energy Unitarity Bounds on the s Matrix,” *Phys. Rev. D* **10** (1974) 1145. [Erratum: *Phys.Rev.D* 11, 972 (1975)].
- [5] R. Aoude and C. S. Machado, “The Rise of SMEFT On-shell Amplitudes,” *JHEP* **12** (2019) 058, [arXiv:1905.11433 \[hep-ph\]](#).
- [6] G. Durieux, T. Kitahara, Y. Shadmi, and Y. Weiss, “The electroweak effective field theory from on-shell amplitudes,” *JHEP* **01** (2020) 119, [arXiv:1909.10551 \[hep-ph\]](#).
- [7] B. Bachu and A. Yellespur, “On-Shell Electroweak Sector and the Higgs Mechanism,” [arXiv:1912.04334 \[hep-th\]](#).
- [8] B. W. Lee, C. Quigg, and H. Thacker, “The Strength of Weak Interactions at Very High-Energies and the Higgs Boson Mass,” *Phys. Rev. Lett.* **38** (1977) 883–885.
- [9] B. W. Lee, C. Quigg, and H. Thacker, “Weak Interactions at Very High-Energies: The Role of the Higgs Boson Mass,” *Phys. Rev. D* **16** (1977) 1519.
- [10] T. Appelquist and M. S. Chanowitz, “Unitarity Bound on the Scale of Fermion Mass Generation,” *Phys. Rev. Lett.* **59** (1987) 2405. [Erratum: *Phys.Rev.Lett.* 60, 1589 (1988)].
- [11] M. S. Chanowitz and M. K. Gaillard, “The TeV Physics of Strongly Interacting W’s and Z’s,” *Nucl. Phys. B* **261** (1985) 379–431.
- [12] F. Maltoni, J. Niczyporuk, and S. Willenbrock, “The Scale of fermion mass generation,” *Phys. Rev. D* **65** (2002) 033004, [arXiv:hep-ph/0106281](#).
- [13] D. A. Dicus and H.-J. He, “Scales of fermion mass generation and electroweak symmetry breaking,” *Phys. Rev. D* **71** (2005) 093009, [arXiv:hep-ph/0409131](#).

- [14] **LHC Higgs Cross Section Working Group** Collaboration, A. David, A. Denner, M. Duehrssen, M. Grazzini, C. Grojean, G. Passarino, M. Schumacher, M. Spira, G. Weiglein, and M. Zanetti, “LHC HXSWG interim recommendations to explore the coupling structure of a Higgs-like particle,” [arXiv:1209.0040 \[hep-ph\]](#).
- [15] T. Corbett, O. J. P. Eboli, and M. C. Gonzalez-Garcia, “Unitarity Constraints on Dimension-Six Operators,” *Phys. Rev. D* **91** no. 3, (2015) 035014, [arXiv:1411.5026 \[hep-ph\]](#).
- [16] T. Corbett, O. Eboli, and M. Gonzalez-Garcia, “Unitarity Constraints on Dimension-six Operators II: Including Fermionic Operators,” *Phys. Rev. D* **96** no. 3, (2017) 035006, [arXiv:1705.09294 \[hep-ph\]](#).
- [17] M. S. Chanowitz and M. K. Gaillard, “Multiple Production of W and Z as a Signal of New Strong Interactions,” *Phys. Lett. B* **142** (1984) 85–90.
- [18] A. Belyaev, A. Oliveira, R. Rosenfeld, and M. C. Thomas, “Multi Higgs and Vector boson production beyond the Standard Model,” *JHEP* **05** (2013) 005, [arXiv:1212.3860 \[hep-ph\]](#).
- [19] A. Falkowski and R. Rattazzi, “Which EFT,” *JHEP* **10** (2019) 255, [arXiv:1902.05936 \[hep-ph\]](#).
- [20] S. Chang and M. A. Luty, “The Higgs Trilinear Coupling and the Scale of New Physics,” *JHEP* **20** (2020) 140, [arXiv:1902.05556 \[hep-ph\]](#).
- [21] C. Vayonakis, “Born Helicity Amplitudes and Cross-Sections in Nonabelian Gauge Theories,” *Lett. Nuovo Cim.* **17** (1976) 383.
- [22] B. Henning, D. Lombardo, M. Riembau, and F. Riva, “Measuring Higgs Couplings without Higgs Bosons,” *Phys. Rev. Lett.* **123** no. 18, (2019) 181801, [arXiv:1812.09299 \[hep-ph\]](#).
- [23] T. Ma, J. Shu, and M.-L. Xiao, “Standard Model Effective Field Theory from On-shell Amplitudes,” [arXiv:1902.06752 \[hep-ph\]](#).
- [24] M. Cepeda *et al.*, *Report from Working Group 2: Higgs Physics at the HL-LHC and HE-LHC*, vol. 7, pp. 221–584. 12, 2019. [arXiv:1902.00134 \[hep-ph\]](#).
- [25] A. Papaefstathiou and K. Sakurai, “Triple Higgs boson production at a 100 TeV proton-proton collider,” *JHEP* **02** (2016) 006, [arXiv:1508.06524 \[hep-ph\]](#).
- [26] C.-Y. Chen, Q.-S. Yan, X. Zhao, Y.-M. Zhong, and Z. Zhao, “Probing triple-Higgs productions via $4b2\gamma$ decay channel at a 100 TeV hadron collider,” *Phys. Rev.* **D93** no. 1, (2016) 013007, [arXiv:1510.04013 \[hep-ph\]](#).

- [27] A. S. Belyaev, P. B. Schaefers, and M. C. Thomas, “Precise test of Higgs boson properties via triple Higgs boson production in vector boson fusion at future colliders,” *Phys. Rev.* **D99** no. 1, (2019) 015030, [arXiv:1801.10157 \[hep-ph\]](#).
- [28] W. Kilian, S. Sun, Q.-S. Yan, X. Zhao, and Z. Zhao, “Multi-Higgs boson production and unitarity in vector-boson fusion at future hadron colliders,” *Phys. Rev. D* **101** no. 7, (2020) 076012, [arXiv:1808.05534 \[hep-ph\]](#).
- [29] D. Stolarski and Y. Wu, “Tree-level Interference in VBF production of Vh ,” [arXiv:2006.09374 \[hep-ph\]](#).
- [30] **ATLAS** Collaboration, G. A. et al, “Combined measurements of Higgs boson production and decay using up to 80 fb^{-1} of proton-proton collision data at $\sqrt{s} = 13$ TeV collected with the ATLAS experiment,” *Phys. Rev. D* **101** no. 1, (2020) 012002, [arXiv:1909.02845 \[hep-ex\]](#).
- [31] J. A. Dror, M. Farina, E. Salvioni, and J. Serra, “Strong tW Scattering at the LHC,” *JHEP* **01** (2016) 071, [arXiv:1511.03674 \[hep-ph\]](#).
- [32] F. Maltoni, L. Mantani, and K. Mimasu, “Top-quark electroweak interactions at high energy,” *JHEP* **10** (2019) 004, [arXiv:1904.05637 \[hep-ph\]](#).
- [33] **ATLAS** Collaboration, “Projections for measurements of Higgs boson cross sections, branching ratios, coupling parameters and mass with the ATLAS detector at the HL-LHC,”. <https://cds.cern.ch/record/2652762>.
- [34] F. Bishara, R. Contino, and J. Rojo, “Higgs pair production in vector-boson fusion at the LHC and beyond,” *Eur. Phys. J. C* **77** no. 7, (2017) 481, [arXiv:1611.03860 \[hep-ph\]](#).
- [35] **ATLAS** Collaboration, G. A. et al, “Search for the $HH \rightarrow b\bar{b}b\bar{b}$ process via vector-boson fusion production using proton-proton collisions at $\sqrt{s} = 13$ TeV with the ATLAS detector,” *JHEP* **07** (2020) 108, [arXiv:2001.05178 \[hep-ex\]](#).
- [36] A. Azatov, R. Contino, G. Panico, and M. Son, “Effective field theory analysis of double Higgs boson production via gluon fusion,” *Phys. Rev. D* **92** no. 3, (2015) 035001, [arXiv:1502.00539 \[hep-ph\]](#).
- [37] C. Englert, F. Krauss, M. Spannowsky, and J. Thompson, “Di-Higgs phenomenology in $t\bar{t}hh$: The forgotten channel,” *Phys. Lett. B* **743** (2015) 93–97, [arXiv:1409.8074 \[hep-ph\]](#).
- [38] G. Li, L.-X. Xu, B. Yan, and C.-P. Yuan, “Resolving the degeneracy in top quark Yukawa coupling with Higgs pair production,” *Phys. Lett. B* **800** (2020) 135070, [arXiv:1904.12006 \[hep-ph\]](#).

- [39] L. Li, Y.-Y. Li, and T. Liu, “Anatomy of the $t\bar{t}h$ Physics at HL-LHC,” *Phys. Rev. D* **101** no. 5, (2020) 055043, [arXiv:1905.03772 \[hep-ph\]](#).